

Nonparametric Bayes Differential Analysis of Multigroup DNA Methylation Data

Chiyu Gu^{*,§}, Veerabhadran Baladandayuthapani^{†,§} and Subharup Guha^{‡,§}

Abstract. DNA methylation datasets in cancer studies are comprised of sample measurements on a large number of genomic locations called cytosine-phosphate-guanine (CpG) sites with complex correlation structures. A fundamental goal of these investigations is the development of statistical techniques that identify disease genomic signatures across multiple patient groups determined by different experimental or biological conditions. We propose *BayesDiff*, a nonparametric Bayesian approach for differential analysis relying on a novel class of first order mixture models called the Sticky Poisson-Dirichlet process or two-restaurant two-cuisine franchise (2R2CF). The BayesDiff methodology flexibly utilizes information from all CpG sites, adaptively accommodating any serial dependence in the data corresponding to the widely varying inter-probe distances, to perform simultaneous inferences about the differential genomic signature of the patient groups. In simulation studies, we demonstrate the effectiveness of the BayesDiff procedure relative to existing statistical techniques for differential DNA methylation. The methodology is applied to analyze a gastrointestinal (GI) cancer DNA methylation dataset that displays both serial correlations and interaction patterns. The results support and complement known aspects of DNA methylation and gene association in upper GI cancers.

Keywords: 2R2CF; First order models; Mixture models; Personalized medicine; Sticky Poisson-Dirichlet process; Two-restaurant two-cuisine franchise.

1 Introduction

Recent advances in array-based and next-generation sequencing (NGS) technologies have revolutionized biomedical research, especially in cancer. The rapid decline in the cost of genome technologies has facilitated the availability of datasets that involve intrinsically different sizes and scales of high throughput data, providing genome-wide, high resolution information about the biology of cancer. In general, a common goal is the identification of differential genomic signatures between groups of samples corresponding to different treatments or biological conditions, e.g., treatment arms, response to adjuvant chemotherapy, tumor subtypes, or cancer stages. The analytic challenges include the high dimensionality of genomic biomarkers or probes, usually in the hundreds of thousands, and the relatively small number of patient samples, usually no more

^{*}Formerly at the University of Missouri. Currently employed at Bayer Crop Science, guchiyu@gmail.com

[†]Department of Biostatistics, University of Michigan, veerab@umich.edu

[‡]Department of Biostatistics, University of Florida, s.guha@ufl.edu

[§]This work was supported by the National Science Foundation under Award DMS-1854003 to SG and Award DMS-1463233 to VB, and by the National Institutes of Health under Grant R01 CA160736 to VB.

than a few hundred. This “small n , large p ” setting results in unstable inferences due to collinearity. Further, there exist complex interaction patterns, such as signaling or functional pathway-based interactions, and genomic or chromosomal location-based serial correlation for high-throughput sequencing data. These data attributes significantly affect the reliability of detecting differential genomic signatures by statistical techniques.

Differential DNA methylation in cancer studies DNA methylation is an important epigenetic mechanism that occurs by the addition of a methyl (CH_3) group to DNA, resulting in the modification of gene functions. It typically occurs at specific genomic locations called cytosine-phosphate-guanine (CpG) sites. Alterations in DNA methylation, e.g., hypomethylation of oncogenes and hypermethylation of tumor suppressor genes, are often associated with the development and progression of cancer (Feinberg and Tycko, 2004). It was previously believed that these alterations occur almost exclusively at promoter regions known as CpG islands, which are chromosomal regions with a high frequency of CpG sites. However, with the advent of high-throughput technologies, it has been shown that a significant proportion of methylation alterations related to cancer do not occur in either promoters or CpG islands (Irizarry et al., 2009), prompting higher resolution, epigenome-wide investigations.

Gastrointestinal (GI) cancer, the most common form of cancer in the U.S. (Siegel et al., 2017), are malignant conditions affecting the digestive system, and are associated with epigenetic alterations (Vedeld et al., 2017). Molecular characterization of the different cancer types, facilitated by the identification of differentially methylated CpG sites, is therefore key to better understanding GI cancer. In the motivating application, we analyze methylation profiles publicly available from The Cancer Genome Atlas (TCGA) project, consisting of 1,224 tumor samples belonging to four GI cancers of the upper digestive tract: stomach adenocarcinoma (STAD), liver hepatocellular carcinoma (LIHC), esophageal carcinoma (ESCA) and pancreatic adenocarcinoma (PAAD). For 485,577 probes, with each probe mapped to a CpG site, DNA methylation levels ranging from 0 (no methylation) to 1 (full methylation) were measured using the Illumina Human Methylation 450 platform.

Figure 1 displays the methylation levels for CpG sites near TP53, a tumor suppressor gene located on chromosome 17. A random subset of the samples was chosen to facilitate an informal visual evaluation. The four sets of colors and shapes of the points represent the four upper GI cancers. Although differential methylation is clearly visible at some CpG sites, the differences are generally subtle, demonstrating the need for sophisticated statistical analyses. An obvious feature is the correlation between the apparent methylation statuses of nearby CpG sites (Eckhardt et al., 2006; Irizarry et al., 2008; Leek et al., 2010). The dependence of proximal CpG sites is also seen in Figure 7 of Supplementary Material, where we find high first order autocorrelations and highly significant tests for serial correlations. Furthermore, the variability of the inter-probe spacings in Figure 1 suggests that the need for modeling distance-based dependencies.

Existing statistical approaches for differential DNA methylation and limitations Numerous frequentist and Bayesian methods have been developed for differential DNA

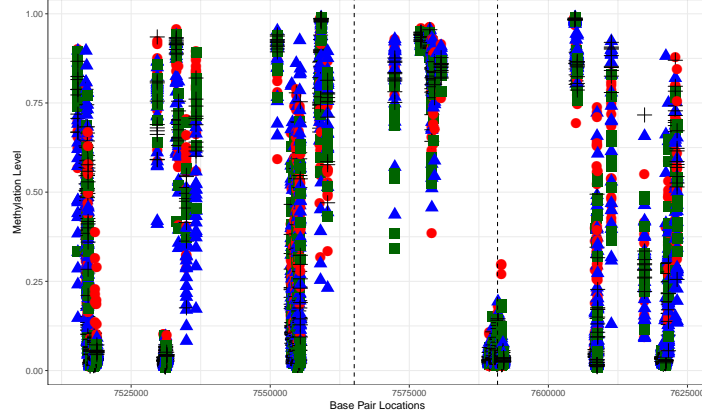


Figure 1: Methylation levels of CpG sites near gene TP53.

methylation, and can be broadly classified into four categories: (i) *Testing-based methods*, such as Illumina Methylation Analyzer (IMA) (Wang et al., 2012), City of Hope CpG Island Analysis Pipeline (COHCAP) (Warden et al., 2013), and BSmooth (Hansen et al., 2012). These methods rely on two-sample or multiple-sample tests for the mean group differences at each CpG site. (ii) *Regression based models*, such as MethylKit (Akalin et al., 2012), bump hunting (Jaffe et al., 2012), Biseq (Hebestreit et al., 2013), and RADMeth (Dolzhenko and Smith, 2014). After applying smoothing or other adjustments, these methods fit individual regression models for each CpG site and test for significance. (iii) *Beta-binomial model-based methods*, such as MOABS (Sun et al., 2014), DSS (Feng et al., 2014), and methylSig (Park et al., 2014). These methods fit separate models for each CpG site. (iv) *Hidden Markov models (HMMs)*, such as MethPipe (Song et al., 2013), Bisulfighter (Saito et al., 2014), and HMM-DM (Yu and Sun, 2016). These methods detect differentially methylated sites based on the inferred hidden states.

The aforementioned methods have several deficiencies. Most methods ignore the strong correlations between neighboring CpG sites or probes, fitting separate models to each probe. This reduces the detection power for the relatively small sample sizes. Additionally, beta-binomial, HMM, and most of the testing-based methods are able to accommodate only two treatments or groups. To handle multiple treatments, they resort to inefficient multiple comparison adjustments. The methods that account for serial dependence (e.g., HMMs) do not adjust for the widely varying distances between the probes, instead assuming uniform inter-site dependencies. The few methods that account for inter-site distances (e.g., Hansen et al., 2012; Jaffe et al., 2012; Hebestreit et al., 2013) rely on ad hoc parameter-tuning procedures that do not adjust for the distinctive data characteristics.

Motivated by these challenges, we propose general and flexible methodology for differential analysis in DNA methylation data, referred to as *BayesDiff*. Rather than fitting a separate model for each CpG site or probe, BayesDiff relies on a global analytical framework for simultaneous inferences on the probes that adapts to the unique data

attributes. To diminish collinearity effects and achieve dimension reduction, the probes are allocated to a smaller, unknown number of latent clusters based on the similarities of probes-specific multivariate parameters. Finally, differential state variables of the probes delineate the genomic signature of the disease to fulfil the main inferential goal.

For realistically modeling the probe-cluster allocation mechanism of DNA methylation profiles, we devise an extension of Poisson Dirichlet processes (PDPs) (Perman et al., 1992) called the *Sticky PDP* (equivalently, the *two-restaurant two-cuisine franchise*). In addition to accounting for long-range biological interactions, this nonparametric process accommodates distance-based serial dependencies of the probes. Additionally, separately for the differential and non-differential probes, it flexibly permits the data to direct the choice between PDPs, and their special case, Dirichlet processes, in finding the best-fitting allocation schemes.

We implement an inferential procedure using a Markov chain Monte Carlo (MCMC) algorithm which is specifically designed for posterior inferences in Sticky PDPs and is scalable to the typically large methylation datasets. Simulation results show that our approach significantly outperforms existing methods for multigroup comparisons in datasets with or without serial correlation. For the motivating TCGA dataset, in addition to confirming known features of DNA methylation and disease-gene associations, the analysis reveals interesting aspects of the biological mechanisms of upper GI cancers.

The rest of the paper is organized as follows. Section 2 describes the BayesDiff approach, with Section 2.1 introducing the Sticky PDP or two-restaurant two-cuisine franchise (2R2CF) for differential DNA methylation. Section 3 outlines a computationally efficient posterior inference procedure for detecting differential probes. For varying noise and correlation levels, Section 4 uses artificial datasets to assess the accuracy of BayesDiff in detecting disease genomic signatures and compares the results with established techniques for DNA methylation data. The motivating upper GI dataset is analyzed using the BayesDiff procedure in Section 5. Finally, conclusions and future related work are discussed in Section 6.

2 The BayesDiff Model

Sequencing technologies measure DNA methylation levels of p biomarkers represented by CpG sites (“probes”) and n matched patient or tissue samples (“individuals”), with p much larger than n . The data belong to the interval $[0, 1]$ and are arranged in an $n \times p$ matrix of proportions, $\mathbf{X} = ((x_{ij}))$, for individuals i and probes j , with the probes sequentially indexed by their genomic locations. The distances between adjacent probes are denoted by e_1, \dots, e_{p-1} , and typically exhibit high variability, e.g., in the upper GI TCGA dataset, the inter-probe distances range from 2 base pairs to 1 megabase pair.

Each individual i is associated with a known experimental or biological condition (“treatment”) denoted by t_i that takes values in $\{1, \dots, T\}$, $T \geq 2$. In the motivating TCGA data, there are $T = 4$ upper GI cancer types. We model the logit transformation of the methylation levels, $z_{ij} = \log(x_{ij}/(1 - x_{ij}))$, as follows:

$$z_{ij} \sim N(\xi_i + \chi_j + \theta_{t_{ij}}, \sigma^2) \quad (2.1)$$

where ξ_i represents the i th subject's random effect, χ_j represents the j th probe's random effect, and θ_{tj} is the random treatment t -probe j interaction effect.

The main inferential goal is the detection of differential probes, i.e., probes j for which the elements of column vector $\boldsymbol{\theta}_j = (\theta_{1j}, \dots, \theta_{Tj})'$ are not all identical. Consequently, we define a binary *differential state variable*, s_j , with $s_j = 1$ indicating that probe j is not differential, and $s_j = 2$ indicating that it is differential:

$$s_j = \begin{cases} 1 & \text{if } \theta_{1j} = \theta_{2j} = \dots = \theta_{Tj}, \\ 2 & \text{otherwise,} \end{cases} \quad (2.2)$$

for $j = 1, \dots, p$. Thus, the key parameters for differential methylation are s_1, \dots, s_p , with the disease genomic signature consisting of the probes with state $s_j = 2$. Motivated by the distance-dependent correlations exhibited by DNA methylation data and the deficiencies of existing statistical approaches noted in Section 1, this paper fosters a novel Bayesian nonparametric framework for the random effects $\boldsymbol{\theta}_1, \dots, \boldsymbol{\theta}_p$ on which the differential state variables depend.

Modeling probe clusters

As mentioned, in addition to high-dimensionality, the analytical challenges posed by DNA methylation datasets include pervasive collinearity caused by dependencies between physically proximal CpG sites or probes. Additionally, there are long-range dependencies between non-adjacent probes due to biological interactions, e.g., signaling or functional pathways. To accommodate dependencies and extract information from the large number of probes, we allocate the p probes to a much smaller number, q , of latent clusters based on the similarities of the random effects $\boldsymbol{\theta}_j$ for probes $j = 1, \dots, p$. We favor clustering to dimension reduction methods such as principal components analysis (PCA). Specifically, because each principal component is a linear combination of all p biomarkers, PCA is less useful in cancer research because of its inability to select features, i.e., probes. By contrast, our approach facilitates biological interpretations by identifying CpG sites relevant to the differential disease genomic signatures.

Suppose that an *allocation variable*, c_j , assigns probe j to one of q latent clusters, where q is unknown. The event $[c_j = k]$ signifies that the j^{th} probe belongs to the k^{th} latent cluster, $k = 1, \dots, q$. We assume that the q clusters are associated with *latent vectors*, $\boldsymbol{\lambda}_1, \dots, \boldsymbol{\lambda}_q$, where the probe-specific random effects and cluster-specific latent vectors have the relation:

$$\boldsymbol{\theta}_j = \boldsymbol{\lambda}_k \quad \text{if } c_j = k. \quad (2.3)$$

That is, all probes within a cluster are assumed to have identical random effects equal to that cluster's latent vector. The differential state variables of the probes, defined in equation (2.2), then become a shared attribute of their parent cluster, and clusters as a whole are either differentially or non-differentially methylated. Further, if probe j belongs to cluster k (i.e., $c_j = k$), then condition $\theta_{1j} = \theta_{2j} = \dots = \theta_{Tj}$ in equation (2.2) is equivalent to $\lambda_{1k} = \lambda_{2k} = \dots = \lambda_{Tk}$, and differential clusters constitute the set

$$\mathcal{D} = \left\{ k : \lambda_{tk} \neq \lambda_{t'k}, \text{ for some } t \neq t', k = 1, \dots, q \right\}. \quad (2.4)$$

Mixture models for allocation Bayesian infinite mixture models are a natural choice for allocating p probes to a smaller, unknown number of latent clusters based on their random effects similarities. Dirichlet processes (Ferguson, 1973a) are arguably the most frequently used infinite mixture models; see Müller and Mitra (2013, chap. 4) for a comprehensive review. The use of Dirichlet processes to achieve dimension reduction in massive datasets has precedence in the literature, albeit in unrelated applications (see Medvedovic et al., 2004; Kim et al., 2006; Dunson et al., 2008; Dunson and Park, 2008; Guha and Baladandayuthapani, 2016). Lijoi, Mena, and Prünster (2007a) advocated the use of Gibbs-type priors (Gnedin and Pitman, 2005) for accommodating more flexible clustering mechanisms, and also demonstrated the utility of Poisson-Dirichlet processes (PDPs) in genomic applications. Formally, the two-parameter PDP (Perman et al., 1992) relies on a discount parameter $d \in [0, 1)$, positive mass parameter α , and T -variate base distribution W , and is denoted by $\mathcal{W}(d, \alpha, W)$. The value $d = 0$ yields a Dirichlet process with mass parameter α and base distribution W . Suppose $\theta_1, \dots, \theta_p$ are distributed as $\mathcal{W}(d, \alpha, W)$. The *stick-breaking representation* of $\mathcal{W}(d, \alpha, W)$ is $\theta_j \stackrel{iid}{\sim} \mathcal{P}$, where random distribution \mathcal{P} is the discrete mixture $\sum_{v=1}^{\infty} \pi_v \delta_{\phi_v}$, with δ_{ϕ_v} denoting a point mass located at the atom $\phi_v \stackrel{iid}{\sim} W$. The random stick-breaking probabilities have the form $\pi_1 = V_1$, and $\pi_h = V_h \prod_{v=1}^{h-1} (1 - V_v)$ for $h > 1$, where $V_h \stackrel{indep}{\sim} \text{beta}(1 - d, \alpha + hd)$. Guha and Baladandayuthapani (2016) introduced VariScan, a technique that utilizes PDPs and Dirichlet processes for clustering, variable selection, and prediction in high-dimensional regression problems in general, and in gene expression datasets in particular. They also demonstrated that PDPs are overwhelmingly favored to Dirichlet processes in gene expression datasets, which typically exhibit no serial correlation.

Limitations of existing mixture models Although the aforementioned mixture models achieve dimension reduction in the large number of probes and account for the long-range biological interactions between non-adjacent probes, a potential drawback is their implicit assumption of apriori probe (i.e., CpG site) exchangeability. Consequently, these techniques cannot account for the serial correlation among CpG sites in methylation data. Infinite HMMs, such as the hierarchical Dirichlet process hidden Markov model (HDP-HMM) (Teh et al., 2006) and Sticky HDP-HMM (Fox et al., 2011), may be utilized to fill this gap. Although these models are a step in the right direction, they have several undesirable features for differential analysis. *First*, the degree of first order dependence is uniform irrespective of the inter-probe distances. This is unrealistic in methylation datasets where the correlation between adjacent probes typically decreases with inter-probe distance (Hansen et al., 2012; Jaffe et al., 2012; Hebestreit et al., 2013). *Second*, an ad hoc exploratory analysis of the GI cancer dataset reveals that the serial correlation in the treatment-probe effects is weaker than the serial dependence between the differential state variables defined in equation (2.2). Although there may not be a biological explanation for this phenomenon, this makes sense from a statistical perspective, because the differential states are binary functions of the treatment-probe interactions; the differential states are more sensitive in detecting first order dependence even when the higher-dimensional (and noisier) treatment-probe interactions show weak or no correlation. This suggests that a hypothetical two-group Markov model, rather than an infinite-group Markov model such as HDP-HMM or Sticky HDP-HMM, would

provide a better fit for the data. *Third*, the range of allocation patterns supported by infinite HMMs is relatively limited. In particular, realistic allocation patterns, such as power law decays in the cluster sizes and large numbers of small-sized clusters, a common feature of cancer datasets (Lijoi et al., 2007b), are assigned relatively small prior probabilities by infinite HMMs.

2.1 Sticky PDP: A Two-restaurant, Two-cuisine Franchise (2R2CF) for Differential Analysis

For the aforementioned reasons, we invent a mixture model called the Sticky PDP. Essentially, this is a cohort of regular PDPs that generates the probe-specific random effects, $\theta_1, \dots, \theta_p$, by switching the generative PDPs at random locations along the probe sequence. Alternatively, the well-known Chinese restaurant franchise (CRF) metaphor for HDP-HMMs and Sticky HDP-HMMs (e.g., Fox et al., 2011) can be generalized to the *two-restaurant two-cuisine franchise* (2R2CF) to provide an equivalent representation of Sticky PDPs appropriate for differential analysis. We present an overview of 2R2CF followed by an in-depth description.

Imagine that a franchise has two restaurants, labeled 1 and 2. Each restaurant consists of two sections, and each section serves a single cuisine consisting of an infinite number of dishes. Section 1 in both the restaurants exclusively serves its customers cuisine 1, whereas section 2 exclusively serves cuisine 2. The *section-cuisine menu*, or a list of available cuisine dishes, is identical at the two restaurants. Although both restaurants serve the two cuisines in their respective sections, restaurant 1 specializes in cuisine 1, and consequently, cuisine 1 is more popular with restaurant 1 patrons. Similarly, cuisine 2 is more popular at restaurant 2 because it specializes in that cuisine. Although every menu item is available at both the restaurants, the relative popularity of each menu item is generally different at the two restaurants.

A succession of p customers, representing the CpG sites or probes, arrive at the franchise, and each customer selects a restaurant followed by a section (equivalently, cuisine) in that restaurant. The waiting times between successive customers, e_1, \dots, e_{p-1} , represent the inter-probe distances. Cuisine 1 symbolizes the non-differential state, and cuisine 2 symbolizes the differential state.

Each restaurant section has an infinite number of tables. A restaurant customer who selects a particular section may either sit at one of the tables already occupied by previous customers in that section, or sit at a new table. All customers who choose an already occupied table are served the same dish, previously chosen from the section-cuisine menu by the first customer who sat at that table. Multiple tables in a section may serve the same dish.

The dish that franchise customer j eats represent their probe-specific random effect, θ_j , of length T . Since cuisine 1 represents the non-differential state, its dishes are characterized by random effects vectors with all T elements equal. Similarly, the cuisine 2 (differential state) dishes are characterized by T -variate random vectors with at least two unequal elements.

By design, if a customer has eaten a dish belonging to cuisine 1 (2), the next customer is more likely to visit restaurant 1 (2), where that cuisine is more popular there. Consequently, a customer tends to select the same cuisine as the previous customer. This model feature accounts for long runs of differential or non-differential states. However, a customer's influence on the next customer diminishes as the time interval separating the two customers increases. That is, the differential statuses of two adjacent probes become statistically independent in the limit as their inter-probe distance grows. The process evolution is graphically illustrated in Figure 2 and discussed below in greater detail.

Cuisine 1 menu. As mentioned, the dishes list on the cuisine 1 menu are characterized by random vectors with all T elements equal. Therefore, they are modeled by *menu distribution* W_1 having the following structure: with $\mathbf{1}_T$ denoting the column vector of T ones,

$$\begin{aligned} W_1 &\stackrel{d}{=} \psi \mathbf{1}_T, \quad \text{where } \psi \in \mathcal{R} \text{ with} \\ \psi &\sim G, \\ G &\sim \mathcal{DP}(\beta, G_0), \quad \text{and} \\ G_0 &= N(\mu_G, \tau_G^2). \end{aligned} \tag{2.5}$$

The symbol $\mathcal{DP}(\beta, G_0)$ denotes a Dirichlet process prior with mass parameter $\beta > 0$ and base distribution G_0 . The stick-breaking representation of the Dirichlet process implies that random distribution G is almost surely discrete, and has the mixture distribution

$$G \stackrel{d}{=} \sum_{v=1}^{\infty} \varpi_v \delta_{\zeta_v}, \quad \text{where } \sum_{v=1}^{\infty} \varpi_v = 1 \text{ and } \zeta_v \stackrel{iid}{\sim} G_0. \tag{2.6}$$

The precise form of the random probabilities, ϖ_v , which depend on mass parameter β , was derived in Sethuraman (1994); see also Ishwaran and James (2003) and Lijoi and Prünster (2010). For natural numbers \mathcal{N} , the set $\mathcal{S}_1 = \{\zeta_v \mathbf{1}_T : v \in \mathcal{N}\}$ then represents the list of available cuisine 1 dishes, and is the support of distribution W_1 . The continuity of base distribution G_0 guarantees that all the menu dishes are unique. The fact that distribution G is discrete has practical consequences for differential analysis: (a) cuisine 1 consists of a countably infinite set, rather than a continuous spectrum, of dishes, and (b) any two section 1 tables may potentially serve the same cuisine 1 dish even if the tables belong to different restaurants.

Cuisine 2 menu. As previously stated, the cuisine dishes characterize the differential state through T -variate random vectors with at least two unequal elements. The menu is modeled by a distribution, W_2 , satisfying two conditions: (i) for similar reasons as the cuisine 1 menu, W_2 is a countably infinite distribution, and (ii) each atom of W_2 has at least two unequal elements. For every $\phi = (\phi_1, \dots, \phi_T)' \in \mathcal{R}^T$, a probability mass function satisfying both conditions can be constructed as follows:

$$W_2(\phi) = \begin{cases} \prod_{t=1}^T G(\phi_t) / (1 - \sum_{v=1}^{\infty} \varpi_v^T) & \text{if } \phi_t \neq \phi_{t'} \text{ for some } t \neq t', \\ 0 & \text{otherwise.} \end{cases} \tag{2.7}$$

where $G(\phi)$ denotes the mass function of distribution G , defined in equation (2.6) and evaluated at $\phi \in \mathcal{R}$. Then, as required, the menu distribution W_2 is discrete and has the countable support,

$$\mathcal{S}_2 = \{(\zeta_{v_1}, \dots, \zeta_{v_T})' : \zeta_{v_t} \neq \zeta_{v_{t'}} \text{ for some integers } v_t \neq v_{t'}, \text{ where } (v_1, \dots, v_T) \in \mathcal{N}^T\}.$$

We observe that the differential and non-differential states communicate through the shared distribution G . When the number of treatments, T , is large, the discreteness of distribution G causes dimension reduction in the T -variate differential state atoms by allowing ties between the atom elements, and resulting in a relatively small number of unique elements within each T -variate atom. When T is large, this model feature facilitates computational savings for the inferential procedure.

Selections made by sequentially arriving 2R2CF customers

For $j \geq 1$, let the restaurant chosen by customer j be denoted by g_j and the cuisine (i.e., section) chosen by customer j be denoted by s_j .

Customer 1. Suppose the first franchise customer, arriving at time 0, selects restaurant $g_1 = 1$ with probability $\rho_1 > 0$ and selects restaurant $g_1 = 2$ with positive probability $\rho_2 = 1 - \rho_1$. For reasons that will become clear, we refer to ρ_1 as the *baseline non-differential proportion* and ρ_2 as the *baseline differential proportion*. Typically, the differential state is less frequent than the non-differential state, and so $\rho_2 < \rho_1$ (i.e., $\rho_2 < 1/2$).

Choice of cuisine s_1 Next, customer 1 selects one of the two cuisine-sections in restaurant g_1 . Recall that each restaurant specializes in the cuisine with the same label, and the specialty cuisine is more popular there. In differential analysis, this is guaranteed by the following assumption. Within restaurant g_j (where $j = 1$ for the first customer), assume customer j selects cuisine 1 with probability

$$\mathcal{Q}_{g_j}(1) = \begin{cases} \rho_1 + \rho_2\gamma & \text{if } g_j = 1, \\ \rho_1 - \rho_1\gamma & \text{if } g_j = 2, \end{cases} \quad (2.8)$$

for a *specialty-cuisine popularity parameter*, $\gamma \in (0, 1]$, determining the degree to which a restaurant's patrons tend to favor its namesake cuisine. Expression (2.8) implies that the customer chooses cuisine 2 in restaurant g_j with probability $\mathcal{Q}_{g_j}(2) = 1 - \mathcal{Q}_{g_j}(1)$.

Choice of table v_1 and dish θ_1 Since the identifiers of the infinite tables belonging to section s_1 of restaurant g_1 are arbitrary, we assume without loss of generality that customer 1 sits at table $v_1 = 1$, and the tables in the restaurant section are assigned consecutive labels as they are occupied by sequentially arriving patrons. Next, customer 1 randomly orders a dish according to menu distribution W_{s_1} , and the dish represents the random effect of the first probe. In other words, $\theta_1 \mid s_1 \sim W_{s_1}$.

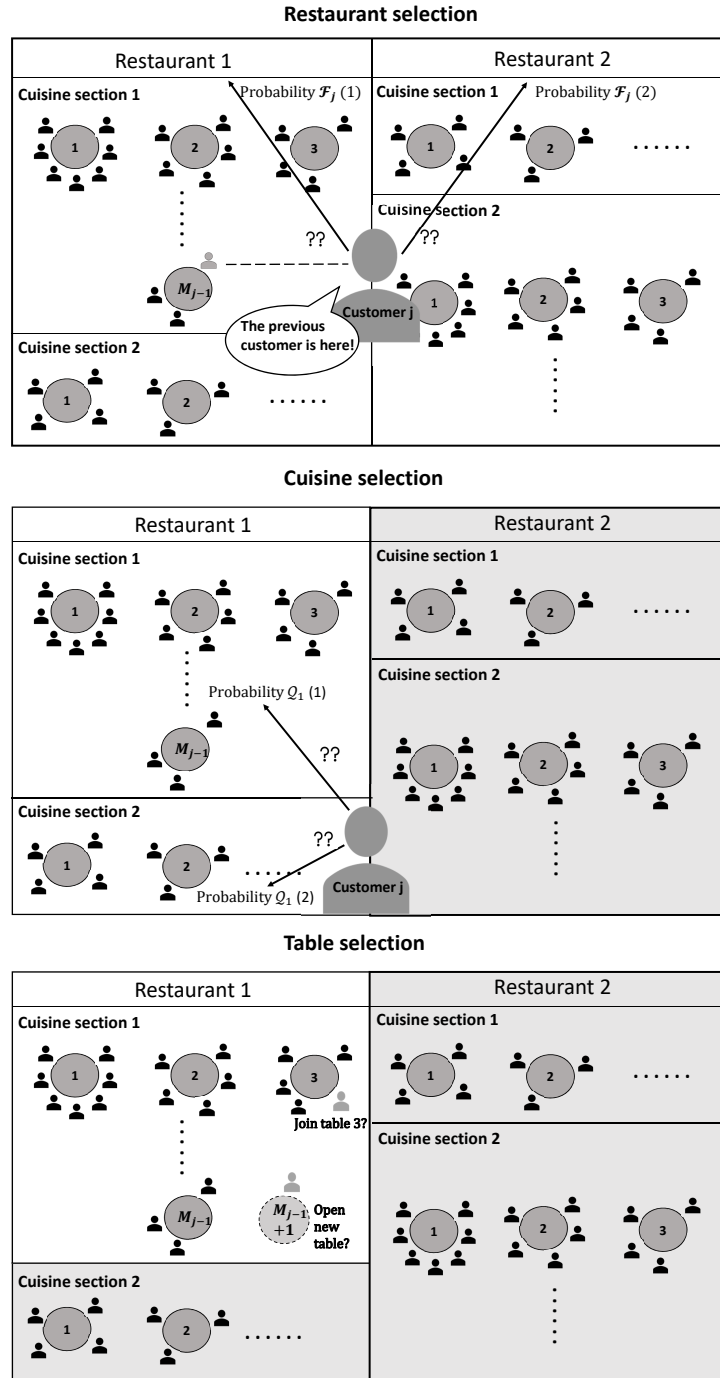


Figure 2: Cartoon representation of the two-restaurant two-cuisine franchise for differential analysis, showing the progressive choice of restaurant, cuisine section, and table by customer j , where $j > 1$. The numbered circles represent the table numbers. See the text in Section 2.1 for a detailed description.

Customer j , where $j > 1$. Unlike customer 1, the *restaurant* choices of the subsequent customers are influenced by the *cuisine* choice of their immediately preceding customer and also by the waiting time separating the two customers. When $j > 1$, suppose customer j arrives at the franchise after a time interval of e_{j-1} after the $(j-1)$ th customer. For a non-negative **dependence parameter** η , time e_{j-1} is first transformed to an **affinity** measure between customer $(j-1)$ and customer j :

$$r_j = \exp(-e_{j-1}/\eta), \quad j > 1, \quad (2.9)$$

belonging to the interval $[0, 1]$ for $\eta > 0$. If $\eta = 0$, affinity r_j is defined as 0 irrespective of the waiting time. As we will see, given the choices of the preceding customer, the affinity influences the behavior of customer j through (2.10) defined below. Additionally, we assume without loss of generality that the waiting times e_1, \dots, e_{p-1} are scaled so that their total equals 1. Since the probes in differential analysis represent CpG sites on a chromosome, it has a unit scaled length if the first probe is located at the chromosomal edge.

Choice of restaurant g_j As previously mentioned, the cuisine s_{j-1} chosen by the $(j-1)$ th customer influences the restaurant choice of the j th customer. Specifically, the selected restaurant

$$g_j \mid s_{j-1} \sim \mathcal{F}_j,$$

where, using the speciality-cuisine popularity parameter γ defined in (2.8), the probability that customer j selects restaurant 1 is

$$\mathcal{F}_j(1) \stackrel{\text{def}}{=} P(g_j = 1 \mid s_{j-1}) = \begin{cases} \rho_1 + \rho_2 r_j / \gamma & \text{if } s_{j-1} = 1, \\ \rho_1 - \rho_1 r_j / \gamma & \text{if } s_{j-1} = 2, \end{cases} \quad (2.10)$$

so that $\mathcal{F}_j(2) = 1 - \mathcal{F}_j(1)$. The idea is illustrated in the top panel of Figure 2, where customer j chooses restaurant 1 with probability $\mathcal{F}_j(1)$ and restaurant 2 with probability $\mathcal{F}_j(2)$. As seen from definition (2.10), if $\eta > 0$, these probabilities depend on the cuisine section s_{j-1} of the previous customer and on the waiting time, e_{j-1} . If $\eta = 0$, on the other hand, the restaurant choices of the customers are independent of one another, and $\mathcal{F}_j(g) = \rho_g$, $g = 1, 2$.

It is easily verified that \mathcal{F}_j is a probability mass function if and only if $r_j/\gamma < 1$. Since the scaled waiting times are bounded above by 1, a globally sufficient condition is $\eta < -1/\log \gamma$. We therefore assume a mixture prior for dependence parameter η :

$$\eta \mid \gamma \sim \frac{1}{2}\delta_0 + \frac{1}{2}\mathcal{H} \cdot \mathcal{I}(\eta < -1/\log \gamma), \quad (2.11)$$

where the second mixture component involves a continuous distribution, \mathcal{H} , restricted to the interval $[0, -1/\log \gamma)$, thereby enforcing the sufficient condition. Speciality-cuisine popularity parameter γ is assigned an independent uniform prior on the unit interval. In our experience, posterior inferences on η are relatively robust to the continuous prior \mathcal{H} provided it is not highly concentrated on a small part of interval $[0, -1/\log \gamma)$.

When $\eta = 0$, we have a *zero-order Sticky PDP*. On the other hand, when $\eta > 0$, we obtain a *first order Sticky PDP*. Some interesting consequences of specification (2.10) are:

1. **Zero-order Sticky PDP:** When $\eta = 0$, each customer independently chooses restaurant 1 (or 2) with probability equal to the baseline proportion of ρ_1 (or ρ_2), and the p customers also act identically.
2. **First order Sticky PDP with e_{j-1}/η large:** Customer j acts approximately independently of the history. Specifically, somewhat similarly to customer 1, customer j chooses restaurant 1 (2) with probability approximately, but not exactly equal to the baseline proportion of ρ_1 (ρ_2). In other words, at large distances, consecutive customers do not appreciably influence each other's choices.
3. **First order Sticky PDP with e_{j-1}/η small:** In the limit as $e_{j-1}/\eta \rightarrow 0$ (e.g., for an infinitesimal inter-probe distance e_{j-1}), the restaurant choice of customer j follows a hidden Markov model.

Since it drives the dependence characteristics of DNA methylation data, posterior inferences on dependence parameter η are of interest. Prior specification (2.11) allows the data to direct the model's order through posterior probability, $P[\eta = 0 \mid \mathbf{X}]$. An MCMC probability estimate is readily available.

Choice of cuisine s_j Within restaurant g_j , customer j selects cuisine-section s_j with distribution \mathcal{Q}_{g_j} , defined earlier in expression (2.8). For a graphical depiction, see the middle panel of Figure 2, where $g_j = 1$. That is, customer j , having already chosen restaurant 1, must now choose a cuisine section. Restaurant 2 has been greyed out because it is no longer accessible to this customer. In the lower panel of Figure 2, we find that the customer has picked cuisine-section 1, i.e., $s_j = 1$, and so, the other restaurant sections are greyed out.

Choice of table v_j Of the previous $(j-1)$ customers, consider the p_{j-1} customers who also chose cuisine-section s_j in restaurant g_j . Then $p_{j-1} = \sum_{l=1}^{j-1} \mathcal{I}(g_l = g_j, s_l = s_j)$. Let the number of tables occupied by these customers in section s_j of restaurant g_j be $M_{j-1} \geq 0$. Recall that all customers seated at a table are served the same dish, chosen from the cuisine menu (in this case, cuisine s_j) by the first customer seated at that table. If $M_{j-1} > 0$, that is, if customer j is not the first patron of the restaurant section, let $\phi_{g_j s_j k}$ denote the dish from cuisine s_j served to the $p_{j-1, k}$ previous customers already seated at table k , where $k = 1, \dots, M_{j-1}$. Clearly, $p_{j-1, k} = \sum_{l=1}^{j-1} \mathcal{I}(g_l = g_j, s_l = s_j, v_l = k)$. Of course, $p_{j-1} = \sum_{k=1}^{M_{j-1}} p_{j-1, k}$. i.e., the number of people who selected section s_j in restaurant g_j before customer j , equals the number of people seated at all currently occupied tables in the restaurant section.

Recall that a new customer may sit at an already occupied table or a new table. Two of these possibilities are illustrated in the lower panel of Figure 2. For a PDP with mass parameter α_{s_j} and discount parameter $d_{s_j} \in [0, 1)$, the predictive distribution of table v_j selected by customer j is specified as

$$P\left(v_j = k \mid p_{j-1,1}, \dots, p_{j-1,M_{j-1}}\right) \propto \begin{cases} p_{j-1,k} - d_{s_j} & \text{if } k = 1, \dots, M_{j-1}, \\ \alpha_{s_j} + M_{j-1}d_{s_j} & \text{if } k = (M_{j-1} + 1), \end{cases} \quad (2.12)$$

where the second line corresponds to customer j sitting at a new table, in which case the updated number of occupied tables becomes $M_j = M_{j-1} + 1$. Otherwise, if customer j sits at a previously occupied table, then $M_j = M_{j-1}$. Obviously, $p_j = p_{j-1} + 1$. Distribution (2.12) implies that customer j is more likely to choose already occupied tables with many occupants, positively reinforcing the selected table's popularity for future customers. The number of occupied tables stochastically increases with the PDP mass and discount parameters.

When PDP discount parameter $d_{s_j} = 0$, we obtain the well-known Pòlya urn scheme for Dirichlet processes (Ferguson, 1973b) for section s_j . PDPs act as effective dimension reduction devices because the random number of occupied tables is much smaller than the number of customers. Specifically, as the number of patrons in the restaurant section grows, i.e., as $p_j \rightarrow \infty$, the number of occupied tables, M_j , is asymptotically equivalent to

$$\begin{cases} \alpha_{s_j} \log p_j & \text{if } d_{s_j} = 0 \\ T_{d_{s_j}, \alpha_{s_j}} p_j^{d_{s_j}} & \text{if } 0 < d_{s_j} < 1 \end{cases} \quad (2.13)$$

for a positive random variable $T_{d_{s_j}, \alpha_{s_j}}$ (Lijoi and Prünster, 2010).

Choice of dish θ_j If customer j sits at a previously occupied table, he or she is served the dish selected by the first customer to occupy that table. Otherwise, if a new table is chosen, customer j picks a dish from menu distribution W_{s_j} . The dish that customer j eats represents probe-specific random effect θ_j and has the distribution:

$$\theta_j \begin{cases} = \phi_{g_j s_j v_j} & \text{if } v_j = 1, \dots, M_{j-1}, \\ \sim W_{s_j} & \text{if } v_j = (M_{j-1} + 1). \end{cases} \quad (2.14)$$

If customer j sits at an already occupied table, then $M_j = M_{j-1}$, and $\theta_j = \phi_{g_j s_j v_j}$ as indicated above. On the other hand, if customer j selects a new table, i.e., if $v_j = (M_{j-1} + 1)$, the number of occupied tables becomes $M_j = M_{j-1} + 1$, and the newly selected dish, $\theta_j = \phi_{g_j s_j M_j} \sim W_{s_j}$ is served to all future customers who sit at table M_j . A consequence of specifications (2.12) and (2.14) is that although each restaurant offers both cuisines and potentially serves every dish, the relative popularity of each dish is restaurant-specific.

The aforementioned process continues for the subsequent franchise customers. As seen in expression (2.10), the cuisine selected by the previous customer influences the restaurant choice of a customer. Additionally, expression (2.8) guarantees that a cuisine is more popular at its namesake restaurant. This makes a customer more likely to select the same cuisine as the previous customer, and facilitates lengthy runs of differential or non-differential states of the probes. In addition to achieving dimension reduction, the proposed Sticky PDP models serial dependencies in the two-state differential status of adjacent probes as a decreasing function of the inter-probe distances.

Latent clusters and their differential states

The notion of latent clusters, introduced earlier in expression (2.3) and forming the basis of the dimension reduction strategy, comprises all probes with identical random

effects. Returning to the 2R2CF metaphor, we find that a cluster is therefore the set of customers eating the same dish. Recall that although customers seated at a table are served the same dish, multiple tables at the two restaurants may serve the same dish because of the shared cuisine menu. Aggregating customers eating the same dishes, irrespective of the restaurant, we obtain the probe-cluster allocation variables c_1, \dots, c_p , and therefore, the random number of latent clusters, q . Additionally, the cuisines determine the common differential states; specifically, the set of distinct cuisine 2 dishes symbolizes the differential clusters, \mathcal{D} , defined in equation (2.4).

From expression (2.13), we expect the number of occupied tables to be much smaller than the number of franchise customers, p . Further, since multiple tables at both restaurants can serve the same dish, the number of latent clusters, q , is smaller than the number of occupied tables. With high probability, this implies that q is much smaller than p .

PDP discount parameter d_2 . Consider the differential state cuisine menu, W_2 , of definition (2.7). It can be shown that when the number of treatments $T \rightarrow \infty$, the individual elements of each T -variate atom of W_2 are asymptotically i.i.d. G , and the differential clusters are not only a posteriori asymptotically identifiable but also consistently detected; refer to Section 4 of [Guha and Baladandayuthapani \(2016\)](#) for a detailed discussion of this remarkable phenomenon in standard PDP settings. Since the differential clusters are often accurately inferred when T and p are large, discount parameter d_2 is given the mixture prior:

$$d_2 \sim \frac{1}{2}\delta_0 + \frac{1}{2}U(0, 1)$$

where $d_2 = 0$ corresponds to a Dirichlet process. This provides the posterior flexibility to choose between a Dirichlet process and a more general PDP for a suitable clustering pattern of the differential probes. Allocation patterns characteristic of non-Dirichlet PDPs, such as power law decays in the cluster sizes and relatively large numbers of small-sized clusters, cause the posterior of parameter d_2 to exclude 0. Allocation patterns more typical of Dirichlet processes, such as exponentially decaying cluster sizes dominated by a few large clusters, result in high posterior probabilities being assigned to 0. A proof of the intrinsically different clusters of Dirichlet processes and PDPs is given in Theorem 2.1 of [Guha and Baladandayuthapani \(2016\)](#).

Since distribution G is discrete, all atoms of T -variate distribution W_2 may not be unique. Indeed, this is common for $T = 2$ treatments. However, as T grows, and provided the number of probes, p , grows at a slower-than-exponential rate as T , the probability that any two allocated atoms are identical rapidly decays to 0. In regression problems unrelated to differential analysis, a similar result was derived for a relatively simple zero-order stochastic process in Section 2.3 of [Guha and Baladandayuthapani \(2016\)](#). We have verified this phenomenon in our simulation studies on differential analysis datasets. In several hundred artificial datasets generated from the Sticky PDP, for $p = 1,500$ probes and T as small as four, no two allocated atoms of W_2 were identical.

PDP discount parameter d_1 . Consider cuisine menu W_1 is defined in (2.5). The flexibility provided by PDP allocation patterns is not necessary for non-differential probes. This is because the allocation patterns of distribution W_1 are driven by univariate parameter ψ in (2.5). In general, the allocations of univariate objects are unidentifiable (e.g., Frühwirth-Schnatter, 2006). Consequently, we set PDP discount parameter $d_1 = 0$, reducing the two PDPs associated with the non-differential state (i.e., section 1 in the two restaurants) to Dirichlet processes.

Other model parameters

Since the essential data features are mostly absorbed by the Sticky PDP model for the random effects θ_j , we can specify simpler parametric models for the remaining terms in relation (2.1). For the subject-specific random effects ξ_1, \dots, ξ_n , we assume i.i.d. $N(0, \tau_\epsilon^2)$ priors. Similarly, appropriate models for the probe-specific parameters χ_1, \dots, χ_p include i.i.d. zero-mean normal distributions, and finite mixture models or HMMs with a finite number of latent states and state-specific normal distributions. An inverse-gamma prior is assigned to parameters σ^2 in (2.1). Appropriate priors are assumed for mass parameters β , α_1 , and α_2 in expressions (2.5) and (2.12). Mean μ_G and variance τ_G^2 of base distribution G_0 in expression (2.5) are given a joint normal-inverse gamma prior. Baseline non-differential proportion ρ_1 is given a uniform prior.

3 Posterior Inference

Due to the analytical intractability of the BayesDiff model, we rely on MCMC methods for posterior inferences and detection of differential probes.

3.1 MCMC Strategy

The model parameters are initialized using naïve estimation techniques and iteratively updated by MCMC techniques until the chain converges. We split the MCMC updates into three blocks. An outline of the MCMC procedure is as follows. Further details can be found in Section 7 of Supplementary Material.

1. **Restaurant-cuisine-table-dish choice $(g_j, s_j, v_j, \theta_j)$ of customer j :** For each probe $j = 1, \dots, p$, we sample the 4-tuple $(g_j, s_j, v_j, \theta_j)$ given the 4-tuples of the other $(p-1)$ probes. This is achieved by proposing a new value of $(g_j, s_j, v_j, \theta_j)$ from a carefully constructed approximation to its full conditional, and by accepting or rejecting the proposed parameters in a Metropolis-Hastings step. The procedure is repeated for all p probes. As discussed in Section 2.1, the probe-cluster allocations c_1, \dots, c_p are immediately available from the restaurant-cuisine-table allocations (g_j, s_j, v_j) of the p probes. Also available are the q latent clusters along with their allocated probes, and the set of differential clusters \mathcal{D} .
2. **Latent vectors $\lambda_1, \dots, \lambda_q$:** There are Tq latent vector elements, not all of which are necessarily distinct because of the Dirichlet process prior on distribu-

tion G . Although the latent vector elements are known from the Block 1 updates, MCMC mixing is considerably improved by updating the latent vector elements conditional on the p probe-cluster allocations. As the calculation in Supplementary Material shows, this is possible by Gibbs sampling.

3. **Remaining model parameters:** Generated by standard MCMC techniques.

Scalability Due to the intensive nature of the one-parameter-at-a-time Gibbs sampling updates in Block 2, the Metropolis-Hastings algorithm of Guha (2010) can be applied to significantly speed up the updates. Relatively to standard Gibbs samplers, ten- to hundred-fold speedups are possible by this fast MCMC strategy. A similar strategy can be applied to obtain order of magnitude speedups for the Block 1 parameters.

3.2 Detection of Differential Probes with FDR Control

Post-processing the MCMC sample, a Bayesian approach for controlling the false discovery rate (FDR) (Newton et al., 2004) is applied for more accurately detecting the differential probes, i.e., the probes j with differential state, $s_j = 2$. Specifically, let q_0 be the nominal FDR level and let ω_j be the posterior probability of probe j being differential, so that $\omega_j = P[s_j = 2 \mid \mathbf{X}]$. An empirical average estimate, $\hat{\omega}_j$, is available from the MCMC sample. To achieve the desired FDR level in calling the differential probes, we first rank all the probes in decreasing order of $\hat{\omega}_j$. Let $\hat{\omega}_{(1)} > \hat{\omega}_{(2)} > \dots > \hat{\omega}_{(p)}$ denote the ordered posterior probability estimates. For each $b = 1, \dots, p$, we calculate as follows the posterior expected FDR resulting from calling the first b probes in decreasing order of $\hat{\omega}_j$:

$$\widehat{\text{FDR}}_b = \frac{\sum_{j=1}^p (1 - \hat{\omega}_j) \mathcal{I}(\hat{\omega}_j \geq \hat{\omega}_{(b)})}{\sum_{j=1}^p \mathcal{I}(\hat{\omega}_j \geq \hat{\omega}_{(b)})} = \frac{\sum_{j=1}^b (1 - \hat{\omega}_{(j)})}{b}, \quad (3.1)$$

where the simplified expression follows from the fact that the $\hat{\omega}_j$'s are sorted. Finally, we pick the largest value of b , denoted by b^* , for which $\widehat{\text{FDR}}_{b^*} < q_0$. A nominal FDR level of q_0 is achieved by labeling as differential the first b^* probes arranged in decreasing order of $\hat{\omega}_j$.

4 Simulation Studies

Using artificial datasets with $T = 5$ treatments, we analyzed the accuracy of BayesDiff in detecting the differentially methylated probes. We also compared the results with established differential methylation procedures and general statistical techniques for multigroup comparisons. Further, we evaluated the ability of the BayesDiff procedure in discovering the complex dependence structure of DNA methylation data.

Generation strategy Proportions representing DNA methylation data were generated using the logit transformation in equation (2.1). The distances between the p probes were

actual sequences of $(p - 1)$ inter-probe distances from the motivating TCGA dataset, scaled to add to 1. In order to capture the complexity of methylation data, such as the existence of multiple latent methylation states (e.g., CpG islands and shores), different read depths across CpGs, and the incomplete conversion of bisulphite sequencing, the generation strategy was partly based on techniques implemented in WGBSSuite, a flexible stochastic simulation tool for generating single-base resolution methylation data (Rackham et al., 2015). However, the generation procedure differed from WGBSSuite in some respects. Specifically, it accommodated more than two treatments ($T > 2$). Additionally, as expected in actual methylation datasets, the generation procedure incorporated serial dependence not only in the methylation states, but also in the differential states of the probes.

The probes-specific read depths were generated as $n_j \stackrel{iid}{\sim} \text{Poisson}(50)$. Unlike Bayes-Diff assumption (2.1), there were no subject-specific random effects in the generation mechanism. Instead, the normal mean of the generated data included additive probe-specific random effects, $\chi_1^{(0)}, \dots, \chi_p^{(0)}$, that were generated as follows:

1. Generate the true methylation status of the probes, denoted by $h_1^{(0)}, \dots, h_p^{(0)}$, using the 4-state *distance-based* HMM of Rackham et al. (2015), with the states respectively representing the methylated, first transit, demethylated, and second transit states.
2. Set the baseline methylation levels for the methylated, (first or second) transit, and demethylated states as $p_{\text{methylated}} = 0.8$, $p_{\text{transit}} = 0.5$, and $p_{\text{un-methylated}} = 0.2$, respectively.
3. For $j = 1, \dots, p$, define the mean probe-specific random effect as follows:

$$\tilde{\chi}_j^{(0)} = \begin{cases} \log\left(\frac{p_{\text{methylated}}}{(1-p_{\text{methylated}})}\right) & \text{if } h_j = 1 \text{ (i.e., methylated state),} \\ \log\left(\frac{p_{\text{transit}}}{(1-p_{\text{transit}})}\right) & \text{if } h_j = 2, 4 \text{ (first or second transit state),} \\ \log\left(\frac{p_{\text{demethylated}}}{(1-p_{\text{demethylated}})}\right) & \text{if } h_j = 3 \text{ (i.e., demethylated state).} \end{cases}$$

4. Independently generate true probe-specific random effects: $\chi_j^{(0)} \sim N(\tilde{\chi}_j^{(0)}, \tau_\chi^2)$ for probe $j = 1, \dots, p$.

Noise and dependence levels We investigated four scenarios corresponding to the combinations of two noise levels and two dependence levels. For each scenario, 20 datasets were independently generated, with each dataset consisting of $p = 500$ probes and $T = 5$ treatments with 4 samples each, i.e., a total to $n = 20$ samples. The low noise level corresponded to true variance parameter $\sigma_0^2 = 0.36$; equivalently, to a signal-to-noise of $R_0^2 \approx 70\%$. The high noise level corresponded to $\sigma_0^2 = 1$ or $R_0^2 \approx 40\%$. The true between-probe dependencies comprised two levels: no serial correlation (i.e., a zero-order Sticky PDP) with $\eta_0 = 0$, and positive serial correlation (i.e., a first order Sticky PDP) with $\eta_0 = 0.004$. Although $\eta_0 = 0.004$ may appear to be small, its value is calibrated to the inter-probe distances; when the distance between two adjacent probes

α_1	α_2	d_2	β	γ	ρ_2	μ_G	τ_G^2	τ_χ^2
20	20	0.33	20	0.9	0.1	0	1	0.1225

Table 1: True parameter values used to generate the artificial datasets.

is equal to the standardized average distance of $\bar{e} = 1/(p-1) = 1/499$, $\eta_0 = 0.004$ gives an affiliation of $r_0 = 0.6$ in equation (2.9). Since the affiliations are bounded above by 1, $\eta_0 = 0.004$ represents fairly high inter-probe dependence. For convenience, we will refer to the two dependence levels as “no-correlation” and “high correlation.” The other model parameters were common for the four scenarios and are displayed in Table 1. Setting a true baseline differential proportion of $\rho_2 = 0.1$ resulted in approximately 10% true differentially methylated CpGs in each dataset.

Posterior inferences Assuming all model parameters to be unknown, each artificial dataset was analyzed using the BayesDiff procedure. The true generation mechanism differed in key respects from the BayesDiff model subsequently used to analyze the data. For example, unlike the 4-state HMM of the generation strategy, the probe-specific random effects χ_j were analyzed using a BayesDiff model that ignored the first order dependence, and instead, relied on a 3-state finite mixture model representing the methylated, transit, and unmethylated states. Additionally, in contrast to the zeroed-out subject-specific random effects during data generation, the BayesDiff procedure assumed that the random effects were i.i.d. normal with zero mean.

To assess the accuracy of BayesDiff in detecting the absence or presence of inter-probe serial correlation, in the no-correlation ($\eta_0 = 0$) situation, we evaluated $\log \left(\frac{P[\eta=0|\mathbf{X}]}{P[\eta>0|\mathbf{X}]} \right)$, the log-Bayes factor comparing zero order to first order Sticky PDPs. In the high correlation ($\eta_0 = 0.004$) situation, we evaluated $\log \left(\frac{P[\eta>0|\mathbf{X}]}{P[\eta=0|\mathbf{X}]} \right)$, the log-Bayes factor comparing first order to zero order Sticky PDPs. Thus, in any scenario, a large positive value of this log-Bayes factor constitutes strong evidence that BayesDiff detects the correct model order.

Although conceptually straightforward, the estimation of Bayes factors requires multiple MCMC runs, even for relatively simple parametric models (Chib, 1995). Basu and Chib (2003) extended the estimation strategy to infinite dimensional models such as Dirichlet processes. However, the computational costs are prohibitively high for big datasets, and multiple MCMC runs for estimating Bayes factors would stretch available computational resources far beyond their present-day limits. Faced with these challenges, we relied on an alternative strategy for estimating the *lower bounds* of log-Bayes factors using a single MCMC run. As it turns out, this is often sufficient to infer the Sticky PDP model orders. Let Θ^- denote all BayesDiff model parameters except η . In the high correlation situation, applying Jensen’s inequality, a lower bound for the corresponding log-Bayes factor is $E \left[\log \left(\frac{P[\eta>0|\mathbf{X}, \Theta^-]}{P[\eta=0|\mathbf{X}, \Theta^-]} \right) \mid \mathbf{X} \right]$. Unlike log-Bayes factors, this lower bound can be easily estimated by an empirical average estimate based on a single MCMC run. In the no-correlation situation, a lower bound for the log-Bayes factor, $\log \left(\frac{P[\eta=0|\mathbf{X}]}{P[\eta>0|\mathbf{X}]} \right)$, can be similarly derived.

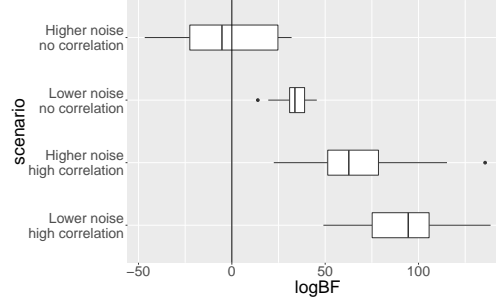


Figure 3: In the simulation study, box plots for the estimated lower bounds of log-Bayes factors in favor of the true model order.

For each of the four generation scenarios, box plots of these estimated lower bounds for the 20 datasets are depicted in Figure 3. Except for the high noise–no-correlation scenario, for which the results were inconclusive, the estimated lower bounds of the log-Bayes factors in favor of the true correlation structure were all positive and large. In the low noise–no-correlation scenario, BayesDiff decisively favored zero-order models, and the smallest lower bound among the 20 datasets was 13.9, corresponding to Bayes factors exceeding $e^{13.9} = 1,088,161$. The 25th percentile of these lower bounds was 30.9, corresponding to Bayes factors exceeding $e^{30.9} = 2.63 \times 10^{13}$. This is strong evidence that the BayesDiff approach is reliable in this scenario. For the high-correlation scenarios, the estimated lower bounds were even higher, showing that BayesDiff overwhelmingly favors first order models when the data are actually serially correlated.

Comparisons with other methods We evaluated the success of the BayesDiff procedure in detecting disease genomic signatures and made comparisons with six well-known procedures. These included some general statistical techniques for multigroup comparisons, namely, one-way analysis of variance (ANOVA) and the Kruskal-Wallis test. We also made comparisons with some methods specially developed for detecting differential methylation in more than two treatments: COHCAP (Warden et al., 2013), methylKit (Akalın et al., 2012), BiSeq (Hebestreit et al., 2013), and RADMeth (Dolzhenko and Smith, 2014). The ANOVA and the Kruskal-Wallis test procedures were applied separately on each probe after applying the inverse-logit transform. Being specifically designed for differential methylation analysis, the COHCAP method was directly applied to the generated proportions of the synthetic data. The remaining three methylation-related methods are designed for bisulfite sequencing, which consists of the total methylation reads for each measured CpG site. For these methods, the methylation reads for each probe was obtained by multiplying the proportion methylation values by the total read. The bandwidth smoothing parameter of the method BiSeq was tuned to optimize the overall detection. For all six methods, the probe-specific p-values were obtained. As recommended by these techniques, the probes whose test p-values were less than the desired significance level were labeled as differential.

We computed the receiver operating characteristic (ROC) curves for differential

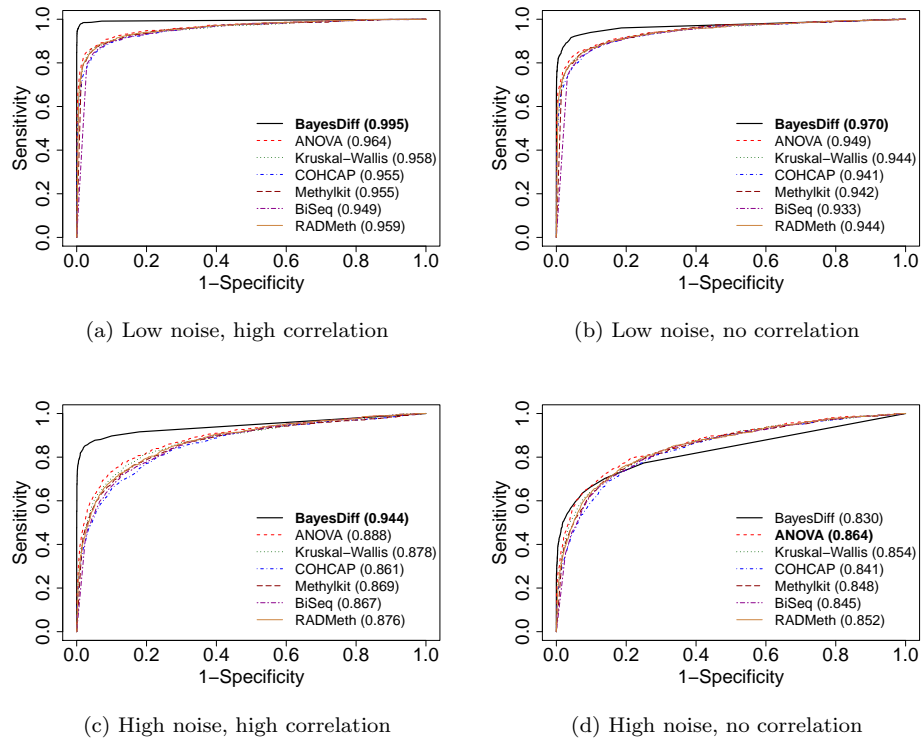


Figure 4: ROC curves, averaged over 20 simulated datasets, for the seven methods and the four simulation scenarios. The numbers in parentheses represent the corresponding AUCs for each method.

probe detection for all seven methods. For a quantitative assessment, we calculated the area under curve (AUC), declaring the method with the largest AUC as the most reliable in each scenario. The ROC curves, averaged over the 20 datasets under each simulation scenario, are shown with the AUCs in Figure 4. In all except the high-noise-no-correlation scenario, BayesDiff uniformly outperformed the other methods, as indicated by the fact that the areas under the ROC curves were greater for BayesDiff. Even in the high-noise-no-correlation scenario, we find that BayesDiff performed better in the low FPR region. As expected, all seven methods had lower accuracies for the higher noise levels. The performance of BayesDiff was significantly better than the competing methods in the high correlation scenarios, suggesting that the incorporation of between-probe dependencies greatly improves its accuracy in situations typical of DNA methylation data.

In addition, since researchers typically focus on small false positive rates (FPRs), that is, small significance levels, we also calculated the measures, AUC_{20} and AUC_{10} . AUC_{20} (AUC_{10}) is defined as the area under the ROC curve multiplied by 5 (10) when the FPR does not exceed 0.2 (0.1). The multiplicative factor ensures that the areas potentially vary between 0 and 1. The three versions of AUC are presented in Table 3 in Supplementary Material. As also seen in Figure 4, Table 3 reveals that in three of the four scenarios, BayesDiff had the largest overall AUC. Furthermore, BayesDiff had vastly improved reliability for low FPRs. For example, consider the low noise-high correlation scenario. The overall AUC for BayesDiff was 0.031 greater than that for ANOVA. In contrast, the gains for BayesDiff, relative to ANOVA, were +0.098 for AUC_{20} and +0.136 for AUC_{10} . The advantages of BayesDiff were even greater relative to the other competing methods. In the high noise-low-correlation scenario, BayesDiff had a relatively low AUC, as mentioned earlier. However, even in this scenario, it had the greatest AUC_{20} and AUC_{10} values among all the methods. Additionally, for a nominal FDR level of $q_0 = 0.05$, the achieved FDR of BayesDiff was between 0 and 0.03 in every dataset and simulation scenario. These results demonstrate the ability of BayesDiff to accurately detect the differential probes even in challenging situations where the FPR is small.

5 Data Analysis

We returned to the motivating DNA methylation dataset consisting of the upper GI cancers: stomach adenocarcinoma (STAD), liver hepatocellular carcinoma (LIHC), esophageal carcinoma (ESCA) and pancreatic adenocarcinoma (PAAD). Applying the BayesDiff procedure, we detected the differentially methylated CpG loci among the cancer types.

Data processing The dataset was obtained from The Cancer Genome Atlas project, which is publicly available through The Genomic Data Commons (GDC) Data Portal (Grossman et al., 2016). The data are available from the Illumina Human Methylation 450 platform for each of 485,577 probes at the CpG sites. At the time of analysis, the dataset consisted of 1,224 tumor samples. The analysis was performed on a gene-by-gene basis. We picked a set of 443 genes involving mutation in at least 5% of the samples.

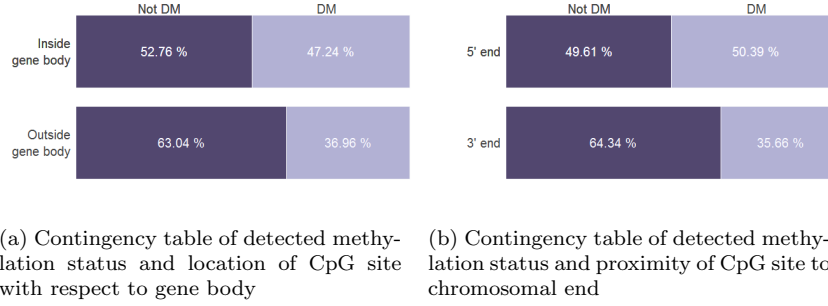


Figure 5: Associations of detected methylation status and position of CpG sites.

To ensure that all CpG sites potentially related to a gene were included in the analysis, we selected all sites located within 50K base pairs outside the gene body, specifically, upstream from the 5' end and downstream from the 3' end. The number of gene-specific CpG sites ranged from 1 to 769, and are displayed in Figure 8(a) of Supplementary Material. As a final preprocessing step, since the methylation patterns of short genes are of lesser interest in cancer investigations, we eliminated the 25 genes mapped to 20 or fewer CpG sites.

Inference procedure The data were analyzed using the proposed BayesDiff approach. Exploratory analyses indicated that a satisfactory fit was obtained by eliminating the probes-specific random effects χ_j in (2.1). The MCMC procedure of Section 3.1 was applied to obtain posterior samples for each gene. For detecting differentially methylated CpG sites, we applied the Bayesian FDR control procedure of Section 3.2 with a nominal FDR of $q_0 = 0.05$.

Results Among the differentially methylated CpG sites detected by our approach, approximately 40.6% of the sites were located outside the gene bodies. Figure 5 displays the associations between detected methylation status and positions of the CpG sites. For our analysis, we have defined “near the 5' (3') end” as the CpG sites located within one-fourth length of the gene body, either inside or outside the gene boundary, and closer to the transcription start (termination) site. Our results indicate that the proportion of differential methylation is higher for CpG sites inside the gene body, and that most differentially methylated loci are situated within the gene body, as is well known from numerous previous studies. However, our analysis also revealed significant amounts of differential methylation outside the gene body. Despite the common belief that DNA methylation analysis should focus on the 5' end region, we found that CpG sites near the 3' ends also display considerable degrees of differential methylation. These findings support the recommendations of Irizarry et al. (2009) that investigations of DNA methylation alteration should be conducted on a higher resolution, epigenome-wide basis.

Among the differentially methylated sites detected by BayesDiff, we estimated the pairwise differences between the random effects associated with the four cancer types.

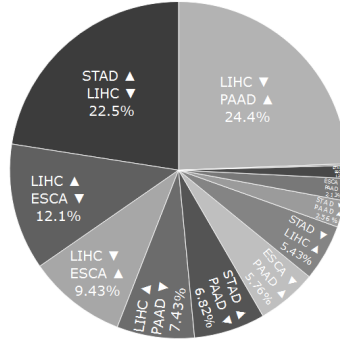


Figure 6: Site-wise summary of the largest pairwise differences of differentially methylated loci among the four upper GI cancer types.

Site-wise summaries of the largest pairwise differences of the cancer-specific effects are plotted in Figure 6. None of the four cancer types displayed consistent hypermethylation or hypomethylation across all the genes or entire chromosomes. However, we found that LIHC is frequently differentially methylated relative to one of the other cancer types, implying that it is the most volatile disease with respect to DNA methylation.

For each gene, Figure 8(b) of Supplementary Material displays 95% credible intervals for lower bounds of log-Bayes factors of a first versus zero-order model, i.e., $\eta = 0$ versus $\eta > 0$ in expression (2.9) for the inter-probe affiliations. Models with first order dependence are overwhelmingly favored for a majority of the genes, suggesting that statistical techniques that do not account for dependence between neighboring CpG sites would be less effective for these data. Figure 9 of Supplementary Material displays the detailed differential methylation pattern for the top two mutated genes, TP53 and TTN. An obvious feature of both the genes is that the detected differential methylation of the CpG sites is highly serially correlated. For gene TP53, there are almost no differentially methylated loci within the gene body. The 3' end region outside the gene body has a cluster of differentially methylated loci, for which cancer type STAD is mostly hypermethylated. The results for gene TTN tell a quite different story: most of the differentially methylated loci are inside the gene body and near the 5' end. Cancer type LIHC is hypomethylated compared to PAAD around the 5' end region, but it is hypermethylated compared to STAD near the 3' end. Finally, genes with at least 90% differentially methylated sites are listed in Table 4 of Supplementary Material, along with the largest pairwise difference between the four cancer types among the differentially methylated loci. The number of CpG sites within each segment is listed in Table 5 of Supplementary Material.

Existing medical literature both supports and complements our findings. For example, hypermethylation of the EDNRB and SLIT2 genes have been found in STAD (Tao et al., 2012). Gene FBN2 was hypermethylated in ESCA (Tsunoda et al., 2009). While

several studies have found that the gene and protein expressions of ABC transporter genes, such as ABCC9, are useful for understanding the prognosis of esophageal cancer (Vrana et al., 2018), we conclude that hypermethylation of ABCC9 is a major difference between cancer types ESCA and LIHC. Gene FLRT2 is a potential tumor suppressor that is hypermethylated and downregulated in breast cancer (Bae et al., 2017). Our results indicate that this gene is also hypermethylated in cancer type STAD versus LIHC. Mutations in SPTA1 gene has been linked with PAAD (Murphy et al., 2013). Our results indicate that hypermethylation of this gene distinguishes PAAD from LIHC.

Accounting for data characteristics In genomic studies, a statistical model should be able to account for the probe-specific means and variances. This is especially important in multiple-testing based approaches where the first two sample moments must be plausibly explained by the fitted model to avoid making misleading biological interpretations (Subramaniam and Hsiao, 2012). From this perspective, certain aspects of the BayesDiff model, such as variance σ^2 a priori unrelated to the mean in expression (2.1), may appear to be restrictive. However, even though the BayesDiff model was not specifically constructed to match data summaries such as sample moments, in practice, the nonparametric nature of the Sticky PDP allows the posterior to flexibly adapt to the features of the data, including sample moments, thereby accounting for mean-variance relationships in a robust manner. For example, consider again the top mutated genes, TP53 and TTN, discussed in Figure 9 of Supplementary Material. The ability of the BayesDiff model to match the sample moments of the gene-specific probes is demonstrated as follows. Given the inter-probe distances, the joint posterior of the BayesDiff parameters induces predictive distributions on the n measurements for each probe. Functionals of these predictive distributions, such as the probe-specific sample moments, are easily estimated by post-processing the MCMC sample. For these two genes, Figure 10 of Supplementary Material shows that the sample moments predicted by BayesDiff closely match the actual first and second sample moments, with correlations exceeding 99% in each plot. Similar results were observed in other datasets.

6 Discussion

DNA methylation data exhibit complex structures due to unknown biological mechanisms and distance-dependent serial correlations among neighboring CpG sites or probes. The identification of differential signatures among different groups of samples is crucial for developing targeted treatments for disease. This paper formulates a flexible approach applicable to multiple treatments called BayesDiff. The technique relies on a novel Bayesian mixture model called the Sticky PDP or the two-restaurant two-cuisine franchise. In addition to allowing simultaneous inferences on the probes, the model accommodates distance-based serial dependence and accounts for the complex interaction patterns commonly observed in cancer data. A computationally efficient MCMC strategy for detecting the differential probes is developed. The success of the BayesDiff procedure in differential DNA methylation, relative to well-established methodologies, is exhibited via simulation studies. The new technique is applied to the motivating TCGA dataset to detect the differential genomic signatures of four upper GI cancers.

The results both support and complement various known facts about the epigenomic differences between these cancer types, while revealing a set of genes exhibiting high proportions of differentially methylated CpG sites. These results emphasize the need for further investigation to better understand the molecular characterizations of different upper GI cancers.

The general methodology is applicable to differential analysis in genomic, epigenomic, transcriptomic, and proteomic datasets. In addition to providing a good fit for the data, a statistical model must be able to account for features of the dataset such as sample moments. The success of the BayesDiff model in this regard is demonstrated in Section 5 for the upper GI dataset. It must be emphasized, however, that there may be other datasets where BayesDiff is less successful in accounting for the data characteristics. This could be due to many reasons, e.g. as the number of probes grows, there is slow asymptotic convergence of the posterior to the true generative process, and so, p is insufficiently large to provide a good match for the data. In such situations, more flexible global transformations (Li et al., 2016) or variance-stabilizing transformations (Durbin et al., 2002) could be used. Alternatively, we could replace the global transformations of the measurements, $z_{ij} = z(x_{ij})$, by local Laplace approximations of exponential family likelihoods through link functions, e.g. binomial likelihoods with logit link for proportions (Zeger and Karim, 1991; Chib and Winkelmann, 2001). In this manner, we could extend the BayesDiff procedure to further improve the model fit and better explain the unique data characteristics.

Going beyond biomedical applications, the generalized form of the Sticky PDP is presented in Section 9 of Supplementary Material. In addition to extending PDPs to discrete time series type data, the generalized formulation offers a diverse palette of parametric and nonparametric models for capturing the distinctive features of data in various applications. The range of models includes Dirichlet processes, PDPs, infinite HMMs, hierarchical Dirichlet process (HDP) (Müller et al., 2004; Teh et al., 2006), finite HMMs, nested Chinese restaurant processes (Blei and Jordan, 2005), nested Dirichlet processes (Rodriguez et al., 2008), and analysis of densities models (Tomlinson and Escobar, 2003).

Ongoing work involves extending the correlation structure to model more sophisticated forms of inter-probe dependence in DNA methylation data. We are currently developing an R package implementing BayesDiff in a parallel computing framework using graphical processing units. The software will be made available for detecting differential genomic signatures in a wide variety of omics datasets. Initial results indicate that dramatic speedups of several orders of magnitude would allow the analysis of user-specified datasets on ordinary personal computers.

Supplementary Material

7 MCMC Strategy

As mentioned in Section 3.1 of the paper, we split the MCMC updates into three blocks. The MCMC procedure for updating Blocks 1 and 2 is described below. Unless otherwise stated, all references to equations, tables, and figures are for the main paper.

1. **Restaurant-cuisine-table-dish choice $(g_j, s_j, v_j, \theta_j)$ of customer j :** For each probe $j = 1, \dots, p$, we sample the 4-tuple $(g_j, s_j, v_j, \theta_j)$ given the 4-tuples of the other $(p-1)$ probes. This is achieved by proposing a new value of $(g_j, s_j, v_j, \theta_j)$ from a carefully constructed approximation to its full conditional, and by accepting or rejecting the proposed 4-tuple of probe-specific parameters in a Metropolis-Hastings step. The procedure is repeated for all p probes to complete the block of MCMC updates.

We give here an intuitive description of the details. Further calculation details are available in Section 8 of Supplementary Material. For the j th probe, $1 < j < p$, the choice of restaurant g_j depends on the triplets of the two immediately adjacent probes. Specifically, as discussed in Section 2.1 and graphically shown in the upper and middle panel of Figure 2, the restaurant selected by a customer depends on the cuisine of the previous customer. Then, within restaurant g_j , the customer chooses cuisine s_j with a restaurant-specific probability. Finally, the customer may either sit an existing table, in which case they must eat the same dish as everyone already sitting at that table, or the customer may open a new table and order a dish from cuisine menu s_j . The generation strategy for table and dish depends on the cuisine, as discussed below.

Cuisine $s_j = 1$ Evaluating the posterior probability of table v_j involves integrating the Gaussian likelihood of column vector $\mathbf{z}_j = (z_{1j}, \dots, z_{nj})'$ with respect to the cuisine 1 menu, i.e., $\theta_j \sim W_1$. Recall that the cuisine 1 menu has the special structure (2.5), allowing its reduction to a univariate quantity distributed as G . This random distribution itself follows a Dirichlet process conditional prior with a base distribution that is a mixture of known atoms (given the 4-tuples of the other probes) and Gaussian distribution G_0 . This conjugate hierarchical structure allows the calculation of table and dish choice for cuisine 1 in computationally closed form.

Cuisine $s_j = 2$ This situation is more complicated because the Gaussian likelihood must be integrated with respect to prior distribution W_2 of the cuisine 2 dishes. Unlike cuisine 1, this is not possible in computationally closed form because menu structure (2.7) cannot be reduced to a univariate quantity. In other words, for cuisine 2 (i.e., the differential state), the Dirichlet process conditional prior for distribution G is non-conjugate.

We utilize an auxiliary variable approach. Given the current set and frequency of atoms of distribution G in the other $(p-1)$ probes, we first compute a finite mixture approximation, G^* , to the Dirichlet process conditional prior for G , as in [Ishwaran and Zarepour \(2002\)](#). Then, using prior (2.7), it is possible to approximate the

posterior probability of customer j joining an existing table or sitting at a new table, irrespective of the dishes. This allows us to generate the table selection, v_j . Finally, we propose the dish, $\theta_j = \phi_{g_j s_j v_j}$. If table v_j is one of the already existing tables, then the customer simply chooses the common, table-specific dish. Otherwise, we sequentially generate from the posterior the T elements representing the new dish. This is done using the corresponding treatment-specific elements of vector $\mathbf{z}_j = (z_{1j}, \dots, z_{nj})'$ and finite mixture G^* , with the restriction that not all T atoms of vector θ_j are equal. The Metropolis-Hasting step compensates for any approximations and produces post-burn-in samples from the BayesDiff model posterior.

Latent clusters As discussed in Section 2.1, the probe-cluster allocations c_1, \dots, c_p are immediately available from the restaurant-cuisine-table allocations (g_j, s_j, v_j) of the p probes. The q latent clusters, along with their allocated probes, and the set of differential clusters \mathcal{D} , are also immediately available.

2. **Latent vectors $\lambda_1, \dots, \lambda_q$:** Since each latent vector is of length T , there are Tq latent vector elements, not all of which are necessarily distinct because of the Dirichlet process prior on distribution G . Although the latent vector elements are available from Block 1, mixing of the MCMC chain is considerably improved by an additional block of updates of the latent vector elements conditional on the p probe-cluster allocations. As the following calculation shows, this can be done by Gibbs sampling.

Since a non-differential cluster's latent vector consists of a single value repeated T times, the number of *distinct* latent vector elements is no more than $(q_1 + Tq_2)$. Given the current probe-cluster allocations, suppose there are m_k probes associated with latent cluster k , where $k = 1, \dots, q$. Let $q_2 = |\mathcal{D}|$ be the number of differential clusters, so that $q_1 = q - q_2$ is the number of non-differential clusters.

Non-differential clusters For these clusters, the latent vector λ_k takes the form, $\lambda_k = \psi_k \mathbf{1}_T$ for some $\psi_k \in \mathcal{R}$. Given the other $(q - 1)$ latent vectors, assumptions (2.5) and (2.7) imply that parameter ψ_k has a Dirichlet process conditional prior. The base distribution of the Dirichlet process is a mixture of a continuous distribution, $G_0 = N(\mu_G, \tau_G^2)$, and the univariate atoms located at the “known” elements of the other $(q - 1)$ latent vectors. The sufficient statistic for ψ_k is

$$\begin{aligned} \bar{y}_k &= \frac{1}{nm_k} \sum_{j=1}^p \sum_{i=1}^n (z_{ij} - \xi_i - \chi_j) \mathcal{I}(c_j = k) \\ &\sim N\left(\psi_k, \frac{\sigma^2}{nm_k}\right) \quad \text{for cluster } k \notin \mathcal{D}. \end{aligned}$$

Since the Dirichlet process conditional prior is conjugate to this normal likelihood, parameter ψ_k could be updated by Gibbs sampling (Escobar, 1994; MacEachern, 1994; Escobar and West, 1995).

Differential clusters For these clusters, some of the T elements of latent vector $\lambda_k = (\lambda_{1k}, \dots, \lambda_{Tk})'$ could be tied, but at least two elements must be unequal.

Denote these restrictions on λ_k by \mathcal{A} . For a treatment t , let the remaining $(T - 1)$ elements of vector λ_k be denoted by λ_{-tk} .

Imagine updating element λ_{tk} assuming that λ_{-tk} and the remaining $(q - 1)$ latent vectors are known. Vector λ_{-tk} and restriction \mathcal{A} imply a possibly restricted support, \mathcal{A}_t , for parameter λ_{tk} . Observe that the support is unrestricted, i.e., $\mathcal{A}_t = \mathcal{R}$, if at least two elements of λ_{-tk} differ. Similarly to non-differential clusters, it can be shown that element λ_{tk} follows a Dirichlet process conditional prior restricted to the support \mathcal{A}_t , and that the base distribution is a mixture of a normal distribution and univariate atoms. The sufficient statistic for latent vector element λ_{tk} is

$$\begin{aligned} \bar{y}_{tk} &= \frac{1}{n_t m_k} \sum_{j=1}^p \sum_{i:t_i=t} (z_{ij} - \xi_i - \chi_j) \mathcal{I}(c_j = k) \\ &\sim N\left(\lambda_{tk}, \frac{\sigma^2}{n_t m_k}\right) \quad \text{for treatment } t = 1, \dots, T, \text{ and cluster } k \in \mathcal{D}, \end{aligned}$$

where n_t is the number of individuals associated with treatment t . The conjugate structure implies that parameter λ_{tk} could be generated from its full conditional by a rejection sampler on set \mathcal{A}_t coupled with standard Gibbs proposals for conjugate Dirichlet processes. In practice, the acceptance rates of the rejection sampler are very high for T as small as 3 or 4, and are nearly 100% for larger T . This is because the posterior probability of support set \mathcal{A}_t tends to 1 as T grows. An intuitive explanation for this asymptotic property is provided in Section 2.1 following the prior specification of discount parameter d_2 .

8 Additional details about Block 1 MCMC updates

In the first block of MCMC updates of Section 3.1, we sample the the set

$$\mathcal{C} = \{(g_j, s_j, v_j, \theta_j) : j = 1, \dots, p\}.$$

We iteratively sample the 4-tuple, $(g_j, s_j, v_j, \theta_j)$, for each probe j via Metropolis-Hastings updates. Specifically, for the j th probe, we propose group (i.e., restaurant) g_j , state (i.e., cuisine) s_j , PDP cluster (i.e., table) label v_j , and random effect (i.e., dish) θ_j , with the proposal distribution approximately equal to the joint posterior of $(g_j, s_j, v_j, \theta_j)$ conditional on the data and all other parameters being equal to the current values. As explained in the paper, since the base measure of the Sticky PDP is discrete and not conjugate to the likelihood, this makes the case of parameter v_j being assigned a new cluster label complicated. To deal with this situation, an auxiliary variable approach is used. Conditional on the current parameter values of the Dirichlet process prior for the latent vector elements, we generate a finite-dimensional approximation, G^* , to the Dirichlet process (Ishwaran and Zarepour, 2002). Since the distribution G^* is discrete, it is characterized by a finite vector of probability masses, π , and the corresponding values of probability mass points, \mathbf{u} . Then, conditional on the auxiliary variables from

G^* , we obtain the quantities needed for the conditional posterior of v_j being assigned a new cluster label in the Metropolis-Hastings algorithm.

More formally, consider probe $j \in \{1, \dots, p\}$. The proposal probabilities for (g_j, s_j, v_j) are as follows:

- For an existing PDP cluster indexed by $v \in \{1, \dots, q_{gs}^{(-j)}\}$,

$$\begin{aligned} Q(g_j = g, s_j = s, v_j = v) &= P(g_j = g, s_j = s, v_j = v \mid \mathbf{z}_j, \mathbf{c}^{(-j)}, \phi_{gsv}, s_{j-1}, \eta, \rho, \gamma, \xi, \chi, \sigma^2) \\ &\propto [\mathbf{z}_j \mid v, s, g, \phi_{gsv}, \xi, \chi, \sigma^2] P(v_j = v \mid \mathbf{c}^{(-j)}, s, g) P(s_j = s \mid g, \gamma, \rho) P(g_j = g \mid s_{j-1}, \eta, \gamma, \rho) \\ &\propto \prod_{i=1}^n \varphi(z_{ij} \mid \phi_{t_i gsv} + \xi_i + \chi_j, \sigma^2) (m_{gsv}^{(-j)} - d_s) \mathcal{Q}_g(s) \mathcal{F}_j(g). \end{aligned} \quad (8.1)$$

- For a new PDP cluster indexed by $v^* = q_{gs}^{(-j)} + 1$,

$$\begin{aligned} Q(g_j = g, s_j = s, v_j = v^*) &= P(g_j = g, s_j = s, v_j = v^* \mid \mathbf{z}_j, \mathbf{c}^{(-j)}, \boldsymbol{\pi}, \mathbf{u}, s_{j-1}, \eta, \rho, \gamma, \xi, \chi, \sigma^2) \\ &\propto [\mathbf{z}_j \mid v^*, s, g, \boldsymbol{\pi}, \mathbf{u}, \xi, \chi, \sigma^2] P(v_j = v^* \mid \mathbf{c}^{(-j)}, s, g) P(s_j = s \mid g, \gamma, \rho) P(g_j = g \mid s_{j-1}, \eta, \gamma, \rho) \\ &\propto \begin{cases} \sum_{l=1}^L \pi_l \left\{ \prod_{i=1}^n \varphi(z_{ij} \mid u_l + \xi_i + \chi_j, \sigma^2) \right\} (\alpha_1 + d_1 q_{g1}^{(-j)}) \mathcal{Q}_g(1) \mathcal{F}_j(g), & \text{if } s = 1, \\ \left\{ \prod_{t=1}^T \sum_{l=1}^L \pi_l \prod_{i:t_i=t} \varphi(z_{ij} \mid u_l + \xi_i + \chi_j, \sigma^2) - \sum_{l=1}^L \pi_l^T \prod_{i=1}^n \varphi(z_{ij} \mid u_l + \xi_i, \sigma^2) \right\} \\ \quad \times (\alpha_2 + d_2 q_{g2}^{(-j)}) \mathcal{Q}_g(2) \mathcal{F}_j(g), & \text{if } s = 2. \end{cases} \end{aligned} \quad (8.2)$$

In expressions (8.1) and (8.2), when $j < p$, superscript $(-j)$ for a variable indicates that the calculation excludes the j th and $(j+1)$ th cluster allocation variables. Specifically, $q_{gs}^{(-j)}$ denotes the number of PDP clusters for group g and state s ; $\mathbf{c}^{(-j)}$ denotes the vector of cluster allocations; $m_{gsv}^{(-j)}$ denotes the cluster membership count for cluster v in the PDP with group g and state s ; $\mathcal{Q}_g(s)$ and $\mathcal{F}_j(g)$ are defined in the paper; $\varphi(\cdot \mid \mu, \sigma^2)$ is the pdf of normal distribution with mean μ and variance σ^2 ; L is the number of distinct mass points in G^* ; u_l denotes the value of distinct mass points in G^* and π_l is the corresponding probability mass. Before calculating the proposal, latent vectors of emptied clusters are removed and cluster labels rearranged so that the largest label is $q_{gs}^{(-j)}$.

The case $v^* = (q_{gs}^{(-j)} + 1)$ corresponds to the case of v_j opening a new cluster. If $v_j = (q_{gs}^{(-j)} + 1)$ has been proposed, then a new random effect of length T is sampled from the posterior distribution based on the n -dimensional observation vector \mathbf{z}_j and the prior G^* characterized by the auxiliary variables, subject to the constraints imposed on the random effects of the differential state s_j .

The Metropolis-Hastings acceptance ratio is computed to decide whether the proposed g_j , s_j and v_j values are accepted. For $j = p$, our proposal density is exactly

the desired conditional posterior, so we always accept the move. For $j < p$, since our proposal density is part of the desired conditional posterior for (g_j, s_j, v_j) , this part cancels out in the acceptance ratio. Therefore, the acceptance ratio only relates to the transition from (g_j, s_j, v_j) to $(g_{j+1}, s_{j+1}, v_{j+1})$, which is

$$r_j = \frac{p\left(g_{j+1}, s_{j+1}, \tilde{v}_{j+1} \mid g_j^*, s_j^*, v_j^*, \phi_{g_{j+1}s_{j+1}\tilde{v}_{j+1}}^*, \mathbf{z}_{j+1}, \mathbf{c}^-, \eta, \xi, \chi, \sigma\right)}{p\left(g_{j+1}, s_{j+1}, v_{j+1} \mid g_j^0, s_j^0, v_j^0, \phi_{g_{j+1}s_{j+1}v_{j+1}}, \mathbf{z}_{j+1}, \mathbf{c}^-, \eta, \xi, \chi, \sigma\right)} \quad (8.3)$$

where g_j^* , s_j^* and v_j^* represent the proposed values; g_j^0 , s_j^0 and v_j^0 are the old values; \tilde{v}_{j+1} denotes v_{j+1} under the proposed variable values (due to possible PDP cluster label change or elimination). Specifically, $\tilde{v}_{j+1} = (q_{g_{j+1}s_{j+1}}^* + 1)$ if it belongs to no existing cluster, where $q_{g_{j+1}s_{j+1}}^*$ is the number of clusters under the proposed variable values and $\phi_{g_{j+1}s_{j+1}\tilde{v}_{j+1}}^*$ is the random effect under the proposed variable values. Both the nominator and the denominator in (8.3) can be calculated using (8.1) and (8.2), and by transposing j to $(j + 1)$.

9 Generalized form of the Sticky PDP

Beyond biomedical applications, a Sticky PDP is defined by the following general properties:

- Property 1: Let set \mathcal{G} contain a countable number of generative *groups*. Each group $g \in \mathcal{G}$ contains a countable number of group-specific regular PDPs. The PDPs are identified by a combination of the group label g and an integer-valued *state*, $s \in \mathcal{S} \subset \mathcal{N}$, the set of natural numbers. That is, the regular PDPs comprising a Sticky PDP have bivariate labels, $(g, s) \in \mathcal{G} \times \mathcal{S}$.
- Property 2: The regular PDPs may have equal or unequal discount parameters, mass parameters, and/or base distributions. For every $(g, s) \in \mathcal{G} \times \mathcal{S}$, let the corresponding PDP be $\mathcal{W}_{gs}(d_s, \alpha_s, W_s)$. With \mathcal{P}_{gs} denoting a random realization of the PDP's stick-breaking distribution, we have

$$\begin{aligned} \mathcal{P}_{gs} &= \sum_{v=1}^{\infty} \pi_{gs v} 1_{\phi_{gs v}} \quad \text{where the } T\text{-variate atoms} \\ \phi_{gs v} &\stackrel{iid}{\sim} W_s, \quad \text{for index } v \in \mathcal{N}, \text{ and probabilities} \\ \pi_{gs 1} &= V_{gs 1}, \quad \pi_{gs h} = V_{gs h} \prod_{v=1}^{h-1} (1 - V_{gs v}), \quad h > 1, \quad \text{with} \\ V_{gs h} &\stackrel{indep}{\sim} \text{beta}(1 - d_s, \alpha_s + h d_s). \end{aligned} \quad (9.1)$$

Notice that base distribution W_s in \mathcal{R}^T is determined by the state s but not group g . On the other hand, the atoms and their associated probabilities in distribution \mathcal{P}_{gs} may depend on both group and state.

If set \mathcal{S} contains multiple states, assume that the set of base distributions $\{W_s : s \in \mathcal{S}\}$ is such that two PDPs associated with unequal states will almost surely have non-intersecting sets of atoms. That is, whenever $s_1^* \neq s_2^*$, the intersection of the random sets of the atoms $\{\phi_{g_1^* s_1^* v}\}_{v=1}^\infty$ and $\{\phi_{g_2^* s_2^* v}\}_{v=1}^\infty$ of stick-breaking distributions $\mathcal{P}_{g_1^* s_1^*}$ and $\mathcal{P}_{g_2^* s_2^*}$ is almost surely empty.

Property 3: For probe $j = 1, \dots, p$, the label of the PDP generating random effect θ_j is denoted by $(g_j, s_j) \in \mathcal{G} \times \mathcal{S}$, and $\theta_j \mid \mathcal{P}_{g_j s_j} \stackrel{\text{indep}}{\sim} \mathcal{P}_{g_j s_j}$. Equivalently, random effect θ_j equals atom $\phi_{g_j s_j v_j}$ with probability $\pi_{g_j s_j v_j}$ for index $v_j \in \mathcal{N}$.

Property 4: Given group g_j for the j^{th} probe, the state of the PDP generating random effect θ_j is randomly selected as follows:

$$s_j \mid g_j \sim \mathcal{Q}_{g_j}$$

where for every $g \in \mathcal{G}$, \mathcal{Q}_g denotes a group-specific probability mass function on the set \mathcal{S} ; thus, $\sum_{s \in \mathcal{S}} \mathcal{Q}_g(s) = 1$.

Property 5: (*Markov property*) For probe $j > 1$, given the variables associated with the preceding probes, group variable g_j has a mass function depending on random vector θ_{j-1} and inter-probe distance e_{j-1} :

$$g_j \sim \mathcal{F}_{\theta_{j-1}, e_{j-1}}$$

where, for every $\theta \in \mathcal{R}^T$ and $e > 0$, $\mathcal{F}_{\theta, e}$ denotes a probability mass function on the set \mathcal{G} , so that $\sum_{g \in \mathcal{G}} \mathcal{F}_{\theta, e}(g) = 1$. For the first probe, group g_1 follows a categorical distribution, \mathcal{F}_0 , on the set \mathcal{G} .

Some examples are presented in Table 2 of Supplementary Material; as suggested by the form of distribution $\mathcal{F}_{\theta, e}$ in the table, the first two models are first order Sticky PDPs. The Sticky PDP corresponding to 2R2CF models used in differential methylation is a special case with two groups and two states. We observe that the first order models displayed in Table 1 are multiple-group, *single-state* models, and that their dependencies are the same irrespective of the inter-probe distances. In contrast, as noted in Consequences 2 and 3 of Section 2.1, the proposed Sticky PDP for differential analysis behaves similarly to two-state hidden Markov models for very small inter-probe distances, and similarly to finite mixture models for relatively large distances. For differential analysis, this offers a key advantage in datasets with widely varying inter-probe distances, as discussed in detail in Section 1. The differential and non-differential probes are allowed to have different cluster allocation patterns depending on the differential status of the adjacent probes. These are some of the features that make Sticky PDPs ideally suited for differential analysis, and are primarily facilitated by the two-group, two-state construct.

Model	\mathcal{G}	$\mathcal{W}_{gs}(d_s, \alpha_s, W_s)$	\mathcal{P}_{gs}	$\mathcal{F}_{\theta,e}$
HDP-HMM	\mathcal{N}	$\mathcal{W}_g(0, \alpha, W)$, countably infinite W	$\sum_{v=1}^{\infty} \pi_{gv} 1_{\phi_v}$	Point mass at $\sum_{v=1}^{\infty} v \cdot \mathcal{I}(\theta = \phi_v)$
Finite HMM	$\{1, \dots, K\}$	$\mathcal{W}_g(0, \alpha, W)$, discrete W with $K < \infty$ atoms	$\sum_{v=1}^K \pi_{gv} 1_{\phi_v}$	Point mass at $\sum_{v=1}^K v \cdot \mathcal{I}(\theta = \phi_v)$
HDP	$\{1, \dots, K\}$	$\mathcal{W}_g(0, \alpha, W)$, countably infinite W	$\sum_{v=1}^{\infty} \pi_{gv} 1_{\phi_v}$	$1_{\{g\}}$, prespecified $g \in \mathcal{G}$
PDP	$\{1\}$	$\mathcal{W}(d, \alpha, W)$	$\sum_{v=1}^{\infty} \pi_v 1_{\phi_v}$	$1_{\{1\}}$
Dirichlet process	$\{1\}$	$\mathcal{W}(0, \alpha, W)$	$\sum_{v=1}^{\infty} \pi_v 1_{\phi_v}$	$1_{\{1\}}$
Finite mixture	$\{1\}$	$\mathcal{W}(0, \alpha, W)$, discrete W with $K < \infty$ atoms	$\sum_{v=1}^K \pi_v 1_{\phi_v}$	$1_{\{1\}}$

Table 2: Examples of Sticky PDPs. Set \mathcal{N} represents the natural numbers. All the above examples correspond to singleton set $\mathcal{S} = \{1\}$ and degenerate distribution $\mathcal{Q}_g = 1_{\{1\}}$. Refer to the description in Section 9 for the notation.

		Low noise		High noise	
		High correlation	No correlation	High correlation	No correlation
AUC	BayesDiff	0.995	0.970	0.944	0.830
	ANOVA	0.964	0.949	0.888	0.864
	Kruskal-Wallis	0.958	0.944	0.878	0.854
	COHCAP	0.955	0.941	0.861	0.841
	Methylkit	0.955	0.942	0.869	0.848
	BiSeq	0.949	0.933	0.867	0.845
	RADMeth	0.959	0.944	0.876	0.852
AUC ₂₀	BayesDiff	0.988	0.926	0.884	0.636
	ANOVA	0.891	0.851	0.684	0.628
	Kruskal-Wallis	0.876	0.833	0.657	0.597
	COHCAP	0.856	0.820	0.602	0.556
	Methylkit	0.858	0.819	0.633	0.579
	BiSeq	0.822	0.781	0.607	0.559
	RADMeth	0.871	0.833	0.639	0.588
AUC ₁₀	BayesDiff	0.985	0.901	0.857	0.565
	ANOVA	0.849	0.804	0.586	0.529
	Kruskal-Wallis	0.827	0.773	0.551	0.493
	COHCAP	0.797	0.751	0.492	0.433
	Methylkit	0.794	0.744	0.523	0.458
	BiSeq	0.726	0.673	0.482	0.424
	RADMeth	0.817	0.775	0.531	0.471

Table 3: Areas under ROC curves for the different methods (rows) under the four simulation scenarios (columns). See the text in the paper for further discussion.

Gene	DM Proportion	Largest Difference	Gene	DM Proportion	Largest Difference
EDNRB	1.00	STAD↑ LIHC↓	SLITRK1	0.96	STAD↑ LIHC↓
PCLO	1.00	PAAD↑ LIHC↓	FLRT2	0.96	STAD↑ LIHC↓
PREX2	1.00	STAD↑ LIHC↓	KCNA1	0.96	STAD↑ LIHC↓
SLIT2	1.00	STAD↑ LIHC↓	TRPA1	0.96	STAD↑ LIHC↓
SLITRK2	1.00	STAD↑ LIHC↓	ADCY8	0.96	STAD↑ LIHC↓
SORCS3	1.00	STAD↑ LIHC↓	CTNNA2	0.95	PAAD↑ LIHC↓
SPHKAP	1.00	ESCA↑ LIHC↓	GRIA2	0.95	STAD↑ LIHC↓
SPTA1	1.00	PAAD↑ LIHC↓	ADGRL3	0.94	PAAD↑ LIHC↓
UNC13C	1.00	PAAD↑ LIHC↓	LRRC7	0.94	STAD↑ LIHC↓
XIRP2	1.00	PAAD↑ LIHC↓	ERBB4	0.93	PAAD↑ LIHC↓
ZNF804B	1.00	STAD↑ LIHC↓	PCDH10	0.93	STAD↑ LIHC↓
TSHZ3	0.97	STAD↑ LIHC↓	SOX11	0.93	STAD↑ LIHC↓
MYO3A	0.97	STAD↑ LIHC↓	NLGN4X	0.93	PAAD↑ LIHC↓
ABCC9	0.97	ESCA↑ LIHC↓	NBEA	0.93	PAAD↑ LIHC↓
EPB41L3	0.97	STAD↑ LIHC↓	CNTN1	0.92	STAD↑ LIHC↓
FBN2	0.97	STAD↑ LIHC↓	GRM5	0.92	PAAD↑ LIHC↓
PCDH17	0.96	STAD↑ LIHC↓	PTPRZ1	0.91	STAD↑ PAAD↓
CDH8	0.96	STAD↑ LIHC↓	EPHA5	0.91	STAD↑ LIHC↓

Table 4: Genes with the overall proportion of differentially methylated CpG sites exceeding 0.9, listed in descending order. The “Largest Difference” column displays which pair-wise difference between the four cancer types is the largest, with the symbol “↑ (↓)” indicating higher (lower) methylation level for one cancer type relative to the other.

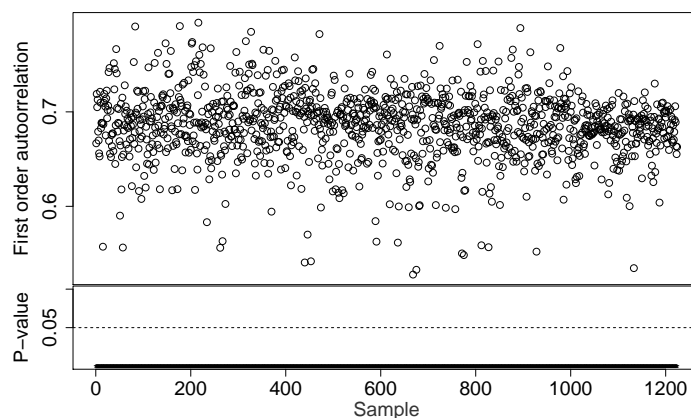


Figure 7: Exploratory analysis of DNA methylation profiles of upper GI cancer samples from TCGA. See the text in the paper for further explanation.

References

- Akalin, A., Kormaksson, M., Li, S., Garrett-Bakelman, F. E., Figueroa, M. E., Melnick, A., and Mason, C. E. (2012). “methylKit: a comprehensive R package for the analysis of genome-wide DNA methylation profiles.” *Genome biology*, 13(10): R87. [3](#), [19](#)
- Bae, H., Kim, B., Lee, H., Lee, S., Kang, H.-S., and Kim, S. J. (2017). “Epigenetically regulated Fibronectin leucine rich transmembrane protein 2 (FLRT2) shows tumor suppressor activity in breast cancer cells.” *Scientific Reports*, 7(1): 272. [24](#)
- Basu, S. and Chib, S. (2003). “Marginal Likelihood and Bayes Factors for Dirichlet Process Mixture Models.” *Journal of the American Statistical Association*, 98(461): 224–235. [18](#)
- Blei, D. M. and Jordan, M. I. (2005). “Variational inference for Dirichlet process mixtures.” *Bayesian Analysis*, 1: 1–23. [25](#)
- Chib, S. (1995). “Marginal Likelihood from the Gibbs Output.” *Journal of the American Statistical Association*, 90(432): 1313–1321. [18](#)
- Chib, S. and Winkelmann, R. (2001). “Markov chain Monte Carlo analysis of correlated count data.” *Journal of Business & Economic Statistics*, 19(4): 428–435. [25](#)
- Dolzhenko, E. and Smith, A. D. (2014). “Using beta-binomial regression for high-precision differential methylation analysis in multifactor whole-genome bisulfite sequencing experiments.” *BMC bioinformatics*, 15(1): 215. [3](#), [19](#)
- Dunson, D. B., Herring, A. H., and Engel, S. M. (2008). “Bayesian selection and clustering of polymorphisms in functionally-related genes.” *Journal of the American Statistical Association*, 103: 534–546. [6](#)

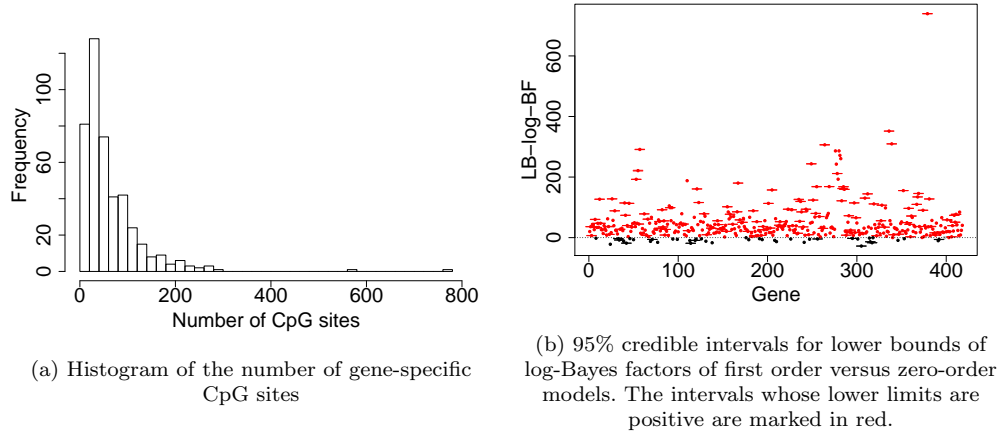
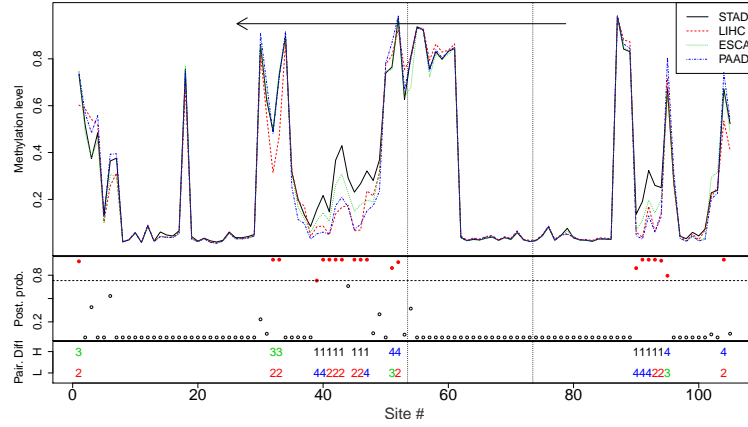


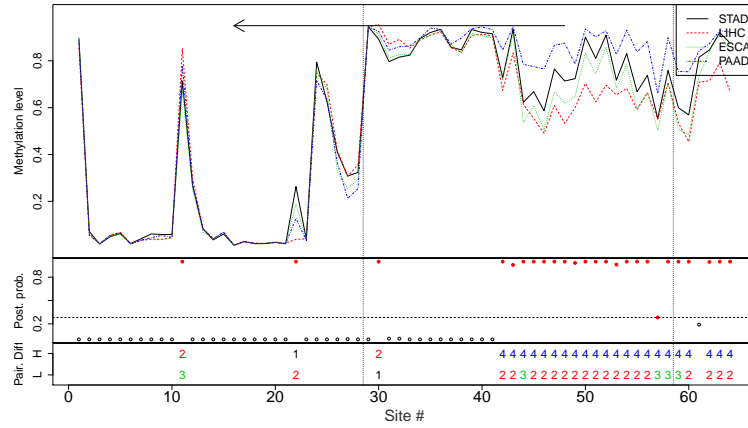
Figure 8: Data analysis plots. See the Section 5 text for further explanation.

Gene	Number of probes	Gene	Number of probes
ABCC9	36	NLGN4X	28
ADCY8	24	PCDH10	30
ADGRL3	35	PCDH17	27
CDH8	26	PCLO	20
CNTN1	25	PREX2	21
CTNNA2	85	PTPRZ1	23
EDNRB	56	SLIT2	29
EPB41L3	34	SLITRK1	26
EPHA5	22	SLITRK2	28
ERBB4	30	SORCS3	39
FBN2	30	SOX11	44
FLRT2	51	SPHKAP	17
GRIA2	20	SPTA1	16
GRM5	25	TRPA1	25
KCNA1	25	TSHZ3	39
LRRC7	34	UNC13C	11
MYO3A	38	XIRP2	19
NBEA	55	ZNF804B	21

Table 5: For the top methylated genes listed in Table 4 of the paper, number of included CpG sites.



(a) Gene TP53



(b) Gene TTN

Figure 9: Detailed differential methylation results for the top 2 mutated genes. For each gene, the upper panel shows the mean methylation levels. The middle panel shows the posterior probabilities of each CpG site being differentially methylated, with solid points representing differential methylation and dashed line denoting the corresponding cutoff value. The lower panel indicates the largest pairwise difference between the 4 cancer types. Symbols 1–4 in the lower panel represent GI cancer types STAD, LIHC, ESCA and PAAD, respectively. The vertical dotted lines represent the gene boundaries. The arrow at the top indicates the transcription direction.

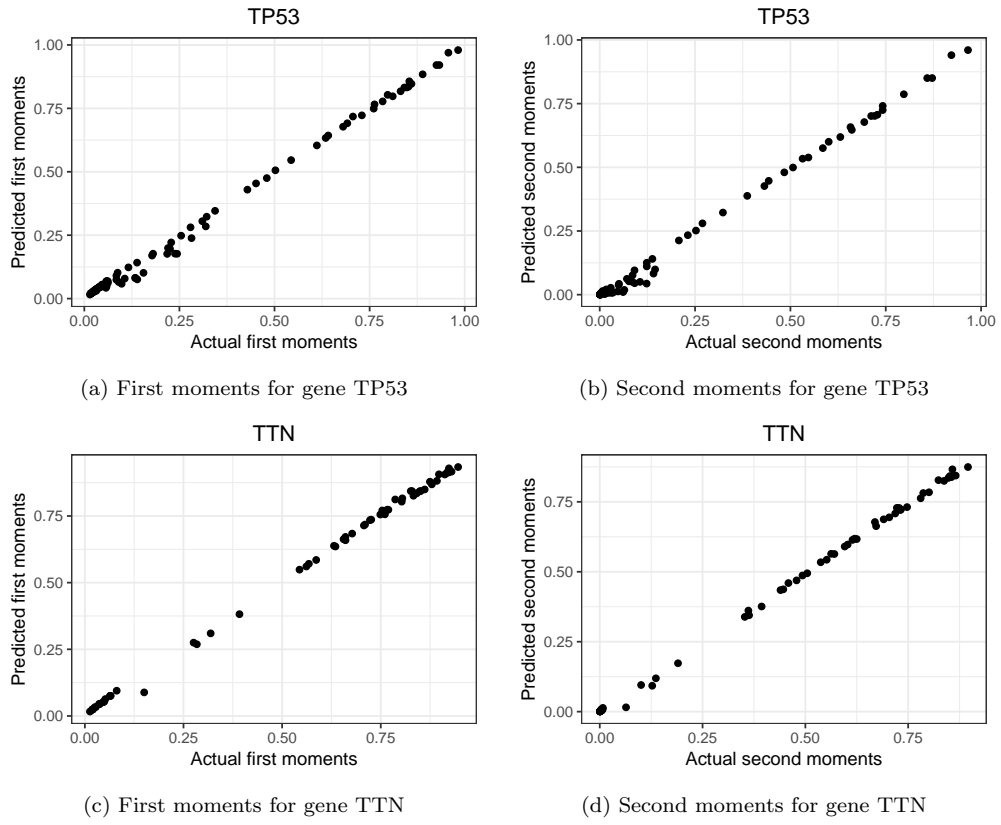


Figure 10: Comparison of predicted and actual sample moments for the 2 top mutated genes

- Dunson, D. B. and Park, J.-H. (2008). “Kernel stick-breaking processes.” *Biometrika*, 95: 307–323. [6](#)
- Durbin, B., Hardin, J., Hawkins, D., and Rocke, D. (2002). “A variance-stabilizing transformation for gene-expression microarray data.” *Bioinformatics*, 18: S105–S110. [25](#)
- Eckhardt, F., Lewin, J., Cortese, R., Rakyan, V. K., Attwood, J., Burger, M., Burton, J., Cox, T. V., Davies, R., Down, T. A., et al. (2006). “DNA methylation profiling of human chromosomes 6, 20 and 22.” *Nature genetics*, 38(12): 1378. [2](#)
- Escobar, M. D. (1994). “Estimating normal means with a Dirichlet process prior.” *Journal of the American Statistical Association*, 89(425): 268–277. [27](#)
- Escobar, M. D. and West, M. (1995). “Bayesian density estimation and inference using mixtures.” *Journal of the american statistical association*, 90(430): 577–588. [27](#)
- Feinberg, A. P. and Tycko, B. (2004). “The history of cancer epigenetics.” *Nature reviews. Cancer*, 4(2): 143. [2](#)
- Feng, H., Conneely, K. N., and Wu, H. (2014). “A Bayesian hierarchical model to detect differentially methylated loci from single nucleotide resolution sequencing data.” *Nucleic acids research*, 42(8): e69–e69. [3](#)
- Ferguson, T. S. (1973a). “A Bayesian analysis of some nonparametric problems.” *The annals of statistics*, 209–230. [6](#)
- (1973b). “A Bayesian Analysis of Some Nonparametric Problems.” *Annals of Statistics*, 1: 209–223. [13](#)
- Fox, E., Sudderth, E., Jordan, M., and Willsky, A. (2011). “The sticky HDP-HMM: Bayesian nonparametric hidden markov models with persistent states.” *Annals of Applied Statistics*, 5: 1020–1056. [6](#), [7](#)
- Frühwirth-Schnatter, S. (2006). *Finite Mixture and Markov Switching Models*. New York: Springer. [15](#)
- Gnedin, A. and Pitman, J. (2005). “Regenerative composition structures.” *Annals of Probability*, 33: 445–479. [6](#)
- Grossman, R. L., Heath, A. P., Ferretti, V., Varmus, H. E., Lowy, D. R., Kibbe, W. A., and Staudt, L. M. (2016). “Toward a shared vision for cancer genomic data.” *New England Journal of Medicine*, 375(12): 1109–1112. [21](#)
- Guha, S. (2010). “Posterior simulation in countable mixture models for large datasets.” *Journal of the American Statistical Association*, 105(490): 775–786. [16](#)
- Guha, S. and Baladandayuthapani, V. (2016). “A Nonparametric Bayesian Technique for High-Dimensional Regression.” *Electronic Journal of Statistics*, 10: 3374–3424. [6](#), [14](#)
- Hansen, K. D., Langmead, B., and Irizarry, R. A. (2012). “BSmooth: from whole genome bisulfite sequencing reads to differentially methylated regions.” *Genome biology*, 13(10): R83. [3](#), [6](#)

- Hebestreit, K., Dugas, M., and Klein, H.-U. (2013). “Detection of significantly differentially methylated regions in targeted bisulfite sequencing data.” *Bioinformatics*, 29(13): 1647–1653. [3](#), [6](#), [19](#)
- Irizarry, R. A., Ladd-Acosta, C., Carvalho, B., Wu, H., Brandenburg, S. A., Jeddeloh, J. A., Wen, B., and Feinberg, A. P. (2008). “Comprehensive high-throughput arrays for relative methylation (CHARM).” *Genome research*, 18(5): 780–790. [2](#)
- Irizarry, R. A., Ladd-Acosta, C., Wen, B., Wu, Z., Montano, C., Onyango, P., Cui, H., Gabo, K., Rongione, M., Webster, M., et al. (2009). “Genome-wide methylation analysis of human colon cancer reveals similar hypo-and hypermethylation at conserved tissue-specific CpG island shores.” *Nature genetics*, 41(2): 178. [2](#), [22](#)
- Ishwaran, H. and James, L. F. (2003). “Generalized weighted Chinese restaurant processes for species sampling mixture models.” *Statist. Sinica*, 13: 1211–1235. [8](#)
- Ishwaran, H. and Zarepour, M. (2002). “Dirichlet prior sieves in finite normal mixtures.” *Statistica Sinica*, 12: 941–963. [26](#), [28](#)
- Jaffe, A. E., Murakami, P., Lee, H., Leek, J. T., Fallin, M. D., Feinberg, A. P., and Irizarry, R. A. (2012). “Bump hunting to identify differentially methylated regions in epigenetic epidemiology studies.” *International journal of epidemiology*, 41(1): 200–209. [3](#), [6](#)
- Kim, S., Tadesse, M. G., and Vannucci, M. (2006). “Variable selection in clustering via Dirichlet process mixture models.” *Biometrika*, 93: 877–893. [6](#)
- Leek, J. T., Scharpf, R. B., Bravo, H. C., Simcha, D., Langmead, B., Johnson, W. E., Geman, D., Baggerly, K., and Irizarry, R. A. (2010). “Tackling the widespread and critical impact of batch effects in high-throughput data.” *Nature reviews. Genetics*, 11(10). [2](#)
- Li, D., Wang, X., Lin, L., and Dey, D. K. (2016). “Flexible link functions in nonparametric binary regression with Gaussian process priors.” *Biometrics*, 72(3): 707–719. [25](#)
- Lijoi, A., Mena, R., and Prünster, I. (2007a). “Bayesian nonparametric estimation of the probability of discovering new species.” *Biometrika*, 94: 769–786. [6](#)
- (2007b). “Controlling the reinforcement in Bayesian nonparametric mixture models.” *Journal of the Royal Statistical Society: Series B (Statistical Methodology)*, 69: 715–740. [7](#)
- Lijoi, A. and Prünster, I. (2010). *Models beyond the Dirichlet process*, 80–136. Cambridge Series in Statistical and Probabilistic Mathematics. [8](#), [13](#)
- MacEachern, S. N. (1994). “Estimating normal means with a conjugate style Dirichlet process prior.” *Communications in Statistics-Simulation and Computation*, 23(3): 727–741. [27](#)
- Medvedovic, M., Yeung, K. Y., and Bumgarner, R. E. (2004). “Bayesian mixture model based clustering of replicated microarray data.” *Bioinformatics*, 20: 1222–1232. [6](#)

- Müller, P. and Mitra, R. (2013). “Bayesian nonparametric inference—why and how.” *Bayesian analysis (Online)*, 8(2). [6](#)
- Müller, P., Quintana, F., and Rosner, G. (2004). “A method for combining inference across related nonparametric Bayesian models.” *Journal of the Royal Statistical Society, Series B*, 66: 735–749. [25](#)
- Murphy, S. J., Hart, S. N., Lima, J. F., Kipp, B. R., Klebig, M., Winters, J. L., Szabo, C., Zhang, L., Eckloff, B. W., Petersen, G. M., et al. (2013). “Genetic alterations associated with progression from pancreatic intraepithelial neoplasia to invasive pancreatic tumor.” *Gastroenterology*, 145(5): 1098–1109. [24](#)
- Newton, M. A., Noueiry, A., Sarkar, D., and Ahlquist, P. (2004). “Detecting differential gene expression with a semiparametric hierarchical mixture method.” *Biostatistics*, 5(2): 155–176. [16](#)
- Park, Y., Figueroa, M. E., Rozek, L. S., and Sartor, M. A. (2014). “MethylSig: a whole genome DNA methylation analysis pipeline.” *Bioinformatics*, 30(17): 2414–2422. [3](#)
- Perman, M., Pitman, J., and Yor, M. (1992). “Size-biased sampling of Poisson point processes and excursions.” *Probability Theory and Related Fields*, 92(1): 21–39. [4](#), [6](#)
- Rackham, O. J., Dellaportas, P., Petretto, E., and Bottolo, L. (2015). “WGBSSuite: simulating whole-genome bisulphite sequencing data and benchmarking differential DNA methylation analysis tools.” *Bioinformatics*, 31(14): 2371–2373. [17](#)
- Rodriguez, A., B., D. D., and Gelfand, A. E. (2008). “The nested Dirichlet process (with discussion).” *Journal of the American Statistical Association*, 103: 1131–1144. [25](#)
- Saito, Y., Tsuji, J., and Mituyama, T. (2014). “Bisulfighter: accurate detection of methylated cytosines and differentially methylated regions.” *Nucleic acids research*, gkt1373. [3](#)
- Sethuraman, J. (1994). “A constructive definition of Dirichlet priors.” *Statistica sinica*, 639–650. [8](#)
- Siegel, R. L., Miller, K. D., and Jemal, A. (2017). “Cancer statistics, 2017.” *CA: A Cancer Journal for Clinicians*, 67(1): 7–30. [2](#)
- Song, Q., Decato, B., Hong, E. E., Zhou, M., Fang, F., Qu, J., Garvin, T., Kessler, M., Zhou, J., and Smith, A. D. (2013). “A reference methylome database and analysis pipeline to facilitate integrative and comparative epigenomics.” *PloS one*, 8(12): e81148. [3](#)
- Subramaniam, S. and Hsiao, G. (2012). “Gene-expression measurement: variance-modeling considerations for robust data analysis.” *Nature immunology*, 13(3): 199–203. [24](#)
- Sun, D., Xi, Y., Rodriguez, B., Park, H. J., Tong, P., Meong, M., Goodell, M. A., and Li, W. (2014). “MOABS: model based analysis of bisulfite sequencing data.” *Genome biology*, 15(2): R38. [3](#)

- Tao, K., Wu, C., Wu, K., Li, W., Han, G., Shuai, X., and Wang, G. (2012). “Quantitative analysis of promoter methylation of the EDNRB gene in gastric cancer.” *Medical Oncology*, 29(1): 107–112. [23](#)
- Teh, Y. W., Jordan, M. I., Beal, M. J., and Blei, D. M. (2006). “Hierarchical Dirichlet processes.” *J. Am. Statist. Ass.*, 101: 1566–1581. [6](#), [25](#)
- Tomlinson, G. and Escobar, M. (2003). “Analysis of Densities.” *Talk given at the Joint Statistical Meeting*, 103: 1131–1144. [25](#)
- Tsunoda, S., Smith, E., De Young, N. J., Wang, X., Tian, Z.-Q., Liu, J.-F., Jamieson, G. G., and Drew, P. A. (2009). “Methylation of CLDN6, FBN2, RBP1, RBP4, TFPI2, and TMEFF2 in esophageal squamous cell carcinoma.” *Oncology reports*, 21(4): 1067–1073. [23](#)
- Vedeld, H. M., Goel, A., and Lind, G. E. (2017). “Epigenetic biomarkers in gastrointestinal cancers: The current state and clinical perspectives.” In *Seminars in cancer biology*. Elsevier. [2](#)
- Vrana, D., Hlavac, V., Brynychova, V., Vaclavikova, R., Neoral, C., Vrba, J., Aujesky, R., Matzenauer, M., Melichar, B., and Soucek, P. (2018). “ABC Transporters and Their Role in the Neoadjuvant Treatment of Esophageal Cancer.” *International journal of molecular sciences*, 19(3): 868. [24](#)
- Wang, D., Yan, L., Hu, Q., Sucheston, L. E., Higgins, M. J., Ambrosone, C. B., Johnson, C. S., Smiraglia, D. J., and Liu, S. (2012). “IMA: an R package for high-throughput analysis of Illumina’s 450K Infinium methylation data.” *Bioinformatics*, 28(5): 729–730. [3](#)
- Warden, C. D., Lee, H., Tompkins, J. D., Li, X., Wang, C., Riggs, A. D., Yu, H., Jove, R., and Yuan, Y.-C. (2013). “COHCAP: an integrative genomic pipeline for single-nucleotide resolution DNA methylation analysis.” *Nucleic acids research*, 41(11): e117–e117. [3](#), [19](#)
- Yu, X. and Sun, S. (2016). “HMM-DM: identifying differentially methylated regions using a hidden Markov model.” *Statistical applications in genetics and molecular biology*, 15(1): 69–81. [3](#)
- Zeger, S. L. and Karim, M. R. (1991). “Generalized linear models with random effects: A Gibbs sampling approach.” *Journal of the American Statistical Association*, 86: 79–86. [25](#)